

# Impact of dipole self-energy on cavity-induced nonadiabatic dynamics

Csaba Fábri,<sup>\*,†,‡</sup> Gábor J. Halász,<sup>¶</sup> Jaroslav Hofierka,<sup>§</sup> Lorenz S. Cederbaum,<sup>§</sup>  
and Ágnes Vibók<sup>\*,‡,||</sup>

<sup>†</sup>*HUN-REN-ELTE Complex Chemical Systems Research Group, P.O. Box 32, H-1518  
Budapest 112, Hungary*

<sup>‡</sup>*Department of Theoretical Physics, University of Debrecen, P.O. Box 400, H-4002  
Debrecen, Hungary*

<sup>¶</sup>*Department of Information Technology, University of Debrecen, P.O. Box 400, H-4002  
Debrecen, Hungary*

<sup>§</sup>*Theoretische Chemie, Physikalisch-Chemisches Institut, Universität Heidelberg, D-69120  
Heidelberg, Germany*

<sup>||</sup>*ELI-ALPS, ELI-HU Non-Profit Ltd, H-6720 Szeged, Dugonics tér 13, Hungary*

E-mail: ficsaba@staff.elte.hu; vibok@phys.unideb.hu

## Abstract

The coupling of matter to the quantized electromagnetic field of a plasmonic or optical cavity can be harnessed to modify and control chemical and physical properties of molecules. In optical cavities, a term known as the dipole self-energy (DSE) appears in the Hamiltonian to assure gauge invariance. The aim of this work is twofold. First, we introduce a method, which has its own merits and complements existing methods, to compute the DSE. Second, we study the impact of the DSE on cavity-induced nonadiabatic dynamics in a realistic system. For that purpose, various matrix elements

of the DSE are computed as functions of the nuclear coordinates and the dynamics of the system after laser excitation is investigated. The cavity is known to induce conical intersections between polaritons, which gives rise to substantial nonadiabatic effects. The DSE is shown to slightly affect these light-induced conical intersections and, in particular, break their symmetry.

## 1 Introduction

Molecular polaritonics is an emerging and rapidly developing field of research.<sup>1-13</sup> The quantized radiation field of optical or plasmonic nanocavities can interact with the dipole moment of molecules, which gives rise to new hybrid light-matter (so-called polaritonic) states, carrying both excitonic (vibronic) and photonic features. Depending on their characteristic frequencies, quantized radiation modes can couple to electronic or vibrational degrees of freedom, leading to vibronic or vibrational polaritons.<sup>8</sup> Over the last decade, an array of experimental<sup>14-25</sup> and theoretical<sup>4,26-53</sup> works have demonstrated that polaritonic states can dramatically modify or even control the physical and chemical properties of molecules. Indeed, the presence of the quantized radiation field can amplify<sup>54</sup> or suppress<sup>27</sup> certain physical processes and even induce new ones. We mention the possibility of strongly varying the rate of spontaneous emission,<sup>55</sup> or influencing the rate of energy transfer<sup>56,57</sup> and charge transfer processes.<sup>58-60</sup> In chemistry, the formation of molecular polaritons offers the possibility of controlling chemical reactions<sup>11,28,61-63</sup> such as photochemical reactivity,<sup>64,65</sup> photoisomerization,<sup>66,67</sup> photodissociation,<sup>68,69</sup> photoionization<sup>70</sup> or photoassociation<sup>71</sup> of molecules.

The strong coupling regime is reached when the rate of energy exchange between cavity photons and the molecule is larger than the rate of photon loss and system dephasing. Strong coupling can be achieved easier with plasmonic nanocavities since plasmonic modes are confined to much smaller volumes than optical cavity photons. However, the lifetime of plasmonic modes is much shorter due to high photon leakage. Modes in plasmonic nanostructures almost always correspond to material excitations (see also Refs. 72-74 for

the quantization of medium-assisted electromagnetic fields). Therefore, the interaction between plasmonic modes and molecules is mostly guided by the Coulomb interaction which is hardly affected by the Power–Zienau–Woolley transformation.<sup>75–77</sup> Consequently, the cavity-molecule interaction can be described with sufficient accuracy by using the usual  $\vec{E} \cdot \vec{d}$  term (electric dipole approximation), without including the dipole self-energy (DSE). In contrast, for electromagnetic fields in optical or Fabry–Pérot cavities, only the transverse component of the vector potential exists, therefore, the DSE term should be included in the interaction term.<sup>78</sup> Hereafter, we will consider the electromagnetic confinement to be an optical cavity. Although strong coupling in optical cavities is currently feasible only for molecular ensembles in experiments, our computations assume a single molecule coupled to an optical cavity in the strong coupling regime.

Light-matter interaction can also induce nonadiabatic effects that are similar in nature to natural nonadiabatic phenomena.<sup>33,79–95</sup> In case of light-induced nonadiabaticity, the radiation field strongly mixes the vibrational, rotational and electronic degrees of freedom of molecules. As a result, light-induced conical intersections (LICIs) are created between polaritonic potential energy surfaces (PESs), leading to the breakdown of the Born–Oppenheimer (BO) approximation.<sup>96</sup> In optical cavities, the DSE term requires the evaluation of matrix elements of the squared dipole moment in the basis of electronic states, which is not available in standard electronic structure program packages. Current techniques for treating the DSE include the resolution-of-identity approach<sup>97</sup> or approximating the DSE term with the square of the ground-state molecular dipole moment for vibrational polaritons.<sup>98</sup> Here, we propose a method that we expect to be more accurate and robust for computing the DSE term. Namely, electronic matrix elements of the squared dipole moment are evaluated directly in the basis of the ground and excited electronic states using the toolbox of electronic structure theory. Thus, no additional approximations are introduced in our treatment on top of the standard ones used in quantum chemistry. To the best of our knowledge, this is the first such implementation treating both the ground and excited electronic states. It is

important to note that a similar approach was employed in Ref. 48 where the ground-state expectation value of the squared dipole moment was obtained directly using Hartree–Fock theory. We also mention that the DSE term is taken into account in quantum-electrodynamic electronic-structure methods.<sup>38,45,99,100</sup>

In this work, we demonstrate how the inclusion of the DSE term affects light-induced nonadiabatic quantum dynamics. Special emphasis is placed on how the position of the LICl changes due to the DSE term and what quantum-dynamical consequences (such as modified conditions for resonant cavity-molecule coupling) the DSE has for a single molecule coupled to an optical cavity mode. The structure of the paper is as follows. Section 2 provides the theoretical description of the cavity-molecule system and the details of electronic structure computations necessary to incorporate the DSE in our procedure. In Section 3 the computational models are described. Section 4 presents and discusses the results of the current study, while conclusion and outlook are given in Section 5.

## 2 Theory

### 2.1 Cavity-molecule system

A single molecule interacting with a cavity mode is described by the Pauli–Fierz Hamiltonian<sup>101</sup>

$$\hat{H} = \hat{H}_0 + \hbar\omega_c \hat{a}^\dagger \hat{a} - g \hat{\mu} \vec{e} (\hat{a}^\dagger + \hat{a}) + \frac{g^2}{\hbar\omega_c} (\hat{\mu} \vec{e})^2 \quad (1)$$

where  $\hat{H}_0$  is the Hamiltonian of the isolated (field-free) molecule,  $\omega_c$  denotes the cavity-mode angular frequency,  $\hat{a}^\dagger$  and  $\hat{a}$  are creation and annihilation operators of the cavity mode,  $\hat{\mu}$  is the electric dipole moment operator of the molecule and  $\vec{e}$  corresponds to the cavity field polarization vector. The cavity-molecule coupling can be characterized by the coupling strength parameter  $g = \sqrt{\frac{\hbar\omega_c}{2\epsilon_0 V}}$  where  $\epsilon_0$  and  $V$  are the permittivity and quantization volume of the cavity, respectively. The last term of  $\hat{H}$  is the so-called dipole self-energy

(DSE).<sup>46,78,102,103</sup>

One way of treating cavity-molecule interactions is the cavity Born–Oppenheimer approach (CBOA).<sup>29,45,46,48,104</sup> In the CBOA, photonic modes are treated nuclear-like and there is a formal equivalence between nuclear and photonic degrees of freedom. In contrast, photonic degrees of freedom can be also grouped with electrons (polaritonic approach) which is particularly useful when multiple electronic states are involved in the dynamics and nonadiabatic effects have to be considered.<sup>105</sup> We focus here on the latter.

If we consider two molecular electronic states (labeled by X and A), the matrix representation of  $\hat{H}$  can be expressed as

$$\hat{H}_{\text{cm}} = \begin{bmatrix} \hat{T} + V_X + Y_X & Y_{XA} & W_X^{(1)} & W_{XA}^{(1)} & \dots \\ Y_{XA} & \hat{T} + V_A + Y_A & W_{XA}^{(1)} & W_A^{(1)} & \dots \\ W_X^{(1)} & W_{XA}^{(1)} & \hat{T} + V_X + Y_X + \hbar\omega_c & Y_{XA} & \dots \\ W_{XA}^{(1)} & W_A^{(1)} & Y_{XA} & \hat{T} + V_A + Y_A + \hbar\omega_c & \dots \\ \vdots & \vdots & \vdots & \vdots & \ddots \end{bmatrix} \quad (2)$$

in the direct product basis of electronic states  $|\alpha\rangle$  ( $\alpha = X, A$ ) and Fock states of the cavity mode  $|n\rangle$  ( $n = 0, 1, 2, \dots$ ).  $\hat{H}_{\text{cm}}$  is an operator in the space of nuclear coordinates,  $\hat{T}$  is the nuclear (rotational-vibrational) kinetic energy operator, while  $V_X$  and  $V_A$  are the ground-state and excited-state molecular potential energy surfaces (PESs). The coupling between the cavity field and the molecular dipole moment operator is described by the operators  $W_\alpha^{(n)} = -g\sqrt{n}\langle\alpha|\hat{\mu}\vec{e}|n\rangle$  ( $\alpha = X, A$ ) and  $W_{XA}^{(n)} = -g\sqrt{n}\langle X|\hat{\mu}\vec{e}|A\rangle$ . Finally, the contribution of the DSE is given by the terms

$$Y_\alpha = \frac{g^2}{\hbar\omega_c} \langle\alpha|(\hat{\mu}\vec{e})^2|\alpha\rangle \quad (3)$$

for  $\alpha = X, A$  and

$$Y_{XA} = \frac{g^2}{\hbar\omega_c} \langle X|(\hat{\mu}\vec{e})^2|A\rangle. \quad (4)$$

In Eq. (2)  $\hat{H}_{\text{cm}}$  is expressed in the so-called diabatic representation (that is, cavity-molecule

coupling terms appear in the potential energy). Polaritonic (hybrid light-matter) PESs are defined as eigenvalues of the potential energy part of  $\hat{H}_{\text{cm}}$  at each nuclear configuration. In what follows, we will assume resonant coupling between electronic states X and A (in other words, the cavity frequency is tuned in resonance with the  $X \rightarrow A$  electronic transition). We retain only the resonantly coupled X and A states and neglect other electronic states which might be necessary to get converged results at higher coupling strengths.<sup>99</sup>

Effects associated with cavity loss are taken into account by the non-Hermitian time-dependent Schrödinger equation (TDSE)<sup>106</sup>

$$i\hbar \frac{\partial |\Phi\rangle}{\partial t} = \left( \hat{H}' - i\frac{\gamma_c}{2} \hat{N} \right) |\Phi\rangle \quad (5)$$

where  $\hat{N} = \hat{a}^\dagger \hat{a}$  and  $\gamma_c$  specifies the cavity decay rate (equivalent to a finite photon lifetime of  $\tau = \hbar/\gamma_c$ ). It is worth noting that since we work in the length gauge (or length representation), photonic and material degrees of freedom are mixed. As a consequence, self-polarization enters the definition of the photon number operator and  $\hat{a}^\dagger \hat{a}$  is not the physical photon number.<sup>78,102</sup> In Eq. (5),  $\hat{H}'$  includes a term which describes the interaction of the molecule with a laser pulse, that is,  $\hat{H}' = \hat{H} - \hat{\mu} \vec{E}(t)$ . The laser pulse is specified by  $|\vec{E}(t)| = E_0 \sin^2(\pi t/T) \cos(\omega t)$  for  $0 \leq t \leq T$  and  $\vec{E}(t) = \vec{0}$  otherwise.  $E_0$ ,  $T$  and  $\omega$  denote the amplitude, length and carrier angular frequency of the pump pulse, respectively. Dissipation during the time evolution of an open quantum system is typically taken into account by using the Lindblad master equation.<sup>107</sup> However, it is shown in Ref. 106 that dissipation can also be described by the non-Hermitian TDSE which provides a viable alternative for the Lindblad master equation. An important merit of the non-Hermitian TDSE formalism is that time evolution can be expressed in terms of the state vector  $|\Psi\rangle$  instead of the density operator (Lindblad master equation), which greatly reduces the computational cost. In case of the non-Hermitian TDSE, the wave function norm decreases over time due to the term  $-i\frac{\gamma_c}{2} \hat{N}$  in Eq. (5). Therefore, in the current work, we choose to set the norm of

the wave function to one at each time propagation step, which is also applied by the stochastic Schrödinger method.<sup>108</sup> In Ref. 47 we found that renormalization of the wave function when propagating the non-Hermitian TDSE tends to give results that agree well with data obtained with the Lindblad master equation.

## 2.2 Electronic structure computations for the dipole self-energy

The projection of  $\hat{\vec{\mu}}$  on the polarization vector can be expressed as

$$\hat{\vec{\mu}}\vec{e} = \sum_{k=x,y,z} \hat{\mu}_k e_k \quad (6)$$

where  $e_k$  are components of the normalized polarization vector  $\mathbf{e} = (e_x, e_y, e_z)$  with  $|\mathbf{e}|^2 = e_x^2 + e_y^2 + e_z^2 = 1$ . With this, the squared dipole projection in the DSE term has the form

$$(\hat{\vec{\mu}}\vec{e})^2 = \sum_{k,l=x,y,z} \hat{\mu}_k \hat{\mu}_l e_k e_l. \quad (7)$$

Eqs. (6) and (7) are general, that is, they describe arbitrary polarization.

As already stated in Section 1, we evaluate the matrix elements of  $(\hat{\vec{\mu}}\vec{e})^2$  in the basis of electronic states  $|\alpha\rangle$  directly. Our approach provides an alternative to existing techniques which are briefly summarized now. One way of computing the DSE is to use the approximation

$$\langle X | \hat{\mu}_k \hat{\mu}_l | X \rangle \approx \langle X | \hat{\mu}_k | X \rangle \langle X | \hat{\mu}_l | X \rangle \quad (8)$$

which has been done for the electronic ground state  $X$ .<sup>98</sup> Another possibility is to insert an approximate resolution of identity in between  $\hat{\mu}_k$  and  $\hat{\mu}_l$ ,

$$\langle \alpha | \hat{\mu}_k \hat{\mu}_l | \alpha' \rangle \approx \sum_{\alpha''} \langle \alpha | \hat{\mu}_k | \alpha'' \rangle \langle \alpha'' | \hat{\mu}_l | \alpha' \rangle \quad (9)$$

where  $|\alpha''\rangle$  denotes electronic states included in the resolution of identity.<sup>97</sup> This approach

might necessitate the computation of many electronic states. This is to be contrasted with the current method, which requires only the electronic states of interest. In what follows, we present both general considerations and a simplified approach which has been used to compute the DSE term in the current work.

### 2.2.1 General approach

In order to incorporate the DSE term in the cavity-molecule Hamiltonian, one has to evaluate matrix elements of the operators  $\hat{\mu}_k \hat{\mu}_l$  in the basis of electronic states (see also Eqs. (3) and (4)). To the best of our knowledge, such matrix elements are not available in standard electronic structure packages. Therefore, we have developed the necessary theory to obtain the desired electronic matrix elements, which is described in this subsection.

The molecular dipole moment operator can be written as the sum of electronic ( $\hat{\mu}_k^e$ ) and nuclear ( $\hat{\mu}_k^n$ ) contributions, that is,

$$\hat{\mu}_k = \hat{\mu}_k^e + \hat{\mu}_k^n = - \sum_{i=1}^{N_e} x_{ik} + \sum_{a=1}^{N_n} Z_a X_{ak} \quad (10)$$

where  $x_{ik}$  and  $X_{ak}$  denote components of electronic and nuclear position vectors, and  $Z_a$  is the charge of nucleus  $a$ . In addition,  $N_e$  and  $N_n$  refer to the number of electrons and nuclei in the (electrically neutral) molecule and atomic units are assumed. Thus, we get

$$\hat{\mu}_k \hat{\mu}_l = \hat{\mu}_k^e \hat{\mu}_l^e + \hat{\mu}_k^e \hat{\mu}_l^n + \hat{\mu}_l^e \hat{\mu}_k^n + \hat{\mu}_k^n \hat{\mu}_l^n \quad (11)$$

where

$$\hat{\mu}_k^e \hat{\mu}_l^e = \sum_{i=1}^{N_e} \sum_{j=1}^{N_e} x_{ik} x_{jl} = \sum_{i=1}^{N_e} x_{ik} x_{il} + \sum_{i=1}^{N_e} \sum_{j \neq i}^{N_e} x_{ik} x_{jl} \quad (12)$$

which includes one-electron and two-electron terms. Using the indistinguishability of elec-

trons, electronic matrix elements of  $\mu_k^e \mu_l^e$  can be expressed as

$$\langle \alpha | \hat{\mu}_k^e \hat{\mu}_l^e | \alpha' \rangle = N_e \langle \alpha | x_{1k} x_{1l} | \alpha' \rangle + N_e(N_e - 1) \langle \alpha | x_{1k} x_{2l} | \alpha' \rangle \quad (13)$$

where  $|\alpha\rangle$  and  $|\alpha'\rangle$  denote molecular electronic states. It is obvious that the first and second terms of Eq. (13) require the one-electron and two-electron reduced density ( $|\alpha\rangle = |\alpha'\rangle$ ) or transition density ( $|\alpha\rangle \neq |\alpha'\rangle$ ) matrices, respectively.

Similarly, matrix elements of  $\hat{\mu}_k^e$  can be cast as

$$\langle \alpha | \hat{\mu}_k^e | \alpha' \rangle = -N_e \langle \alpha | x_{1k} | \alpha' \rangle \quad (14)$$

where only the one-electron reduced (transition) density matrix is needed. With Eqs. (13) and (14), we get

$$\langle \alpha | \hat{\mu}_k \hat{\mu}_l | \alpha' \rangle = \langle \alpha | \hat{\mu}_k^e \hat{\mu}_l^e | \alpha' \rangle + \langle \alpha | \hat{\mu}_k^e | \alpha' \rangle \hat{\mu}_l^n + \langle \alpha | \hat{\mu}_l^e | \alpha' \rangle \hat{\mu}_k^n + \hat{\mu}_k^n \hat{\mu}_l^n \delta_{\alpha\alpha'} \quad (15)$$

which can be evaluated employing any electronic structure method which provides the one-electron and two-electron reduced (transition) density matrices.

Another way of obtaining the expectation value of  $\hat{\mu}_k \hat{\mu}_l$  is to consider the Hamiltonian

$$\hat{H}(\lambda) = \hat{H}_0 + \lambda \hat{\mu}_k \hat{\mu}_l \quad (16)$$

where the molecular Hamiltonian  $\hat{H}_0$  is perturbed by the operator  $\hat{\mu}_k \hat{\mu}_l$  ( $\lambda$  is the perturbation parameter). Within the framework of this perturbation-based formalism it can be shown that the expectation value of  $\hat{\mu}_k \hat{\mu}_l$  over the unperturbed electronic wave function  $|\alpha(0)\rangle$  equals

$$\langle \alpha(0) | \hat{\mu}_k \hat{\mu}_l | \alpha(0) \rangle = \left. \frac{dE(\lambda)}{d\lambda} \right|_{\lambda=0} \quad (17)$$

where  $E(\lambda)$  is the perturbation-dependent energy satisfying  $\hat{H}(\lambda)|\alpha(\lambda)\rangle = E(\lambda)|\alpha(\lambda)\rangle$ . Eq.

(17) is also known as the Hellmann–Feynman theorem<sup>109</sup> which can be extended to account for degenerate states.<sup>110</sup> The Hellmann–Feynman approach is particularly useful if not all wave function parameters are optimized by the variational principle.<sup>109</sup>

### 2.2.2 Simplified approach

In the current work, the excited state (A) is obtained by the configuration interaction singles (CIS) method.<sup>111</sup> Using spin adaptation, singlet and triplet excited states can be computed separately by diagonalizing the singlet and triplet blocks of the CIS Hamiltonian matrix.<sup>111</sup> The singlet block of the CIS Hamiltonian reads

$$H_{ia,jb} = (\epsilon_a - \epsilon_i)\delta_{ij}\delta_{ab} + 2\langle ij|ab\rangle - \langle ia|jb\rangle \quad (18)$$

where  $i, j$  and  $a, b$  label occupied and virtual spatial molecular orbitals (MOs), respectively. Moreover,  $\epsilon_a$  and  $\epsilon_i$  are MO energies, while  $\langle ij|ab\rangle$  and  $\langle ia|jb\rangle$  refer to two-electron (Coulomb) integrals in the basis of canonical MOs using physicist’s notation (1212). This way, CIS amplitudes  $c_{ia}$  and excitation energies  $\Delta E_{\text{CIS}}$  can be found by solving the eigenvalue equation

$$\sum_j^{\text{occ}} \sum_b^{\text{virt}} H_{ia,jb} c_{jb} = \Delta E_{\text{CIS}} c_{ia}. \quad (19)$$

The CIS energies of excited states are given by  $E_{\text{CIS}} = E_{\text{RHF}} + \Delta E_{\text{CIS}}$  where  $E_{\text{RHF}}$  is the ground-state restricted Hartree–Fock (RHF) energy, while the singlet CIS wave functions assume the form

$$|\Psi_{\text{CIS}}\rangle = \frac{1}{\sqrt{2}} \sum_i^{\text{occ}} \sum_a^{\text{virt}} c_{ia} \left( |\Phi_{i\uparrow}^{a\uparrow}\rangle + |\Phi_{i\downarrow}^{a\downarrow}\rangle \right) \quad (20)$$

where  $|\Phi_{i\sigma}^{a\sigma}\rangle$  denote singly-excited Slater determinants with an electron of spin  $\sigma = \uparrow, \downarrow$  promoted to the virtual MO  $|a\rangle$  from the occupied MO  $|i\rangle$ . We emphasize that, due to Brillouin’s theorem, singly-excited determinants do not mix with the ground-state RHF determinant.<sup>109</sup> As a consequence, the ground state at the CIS level of theory equals the RHF reference.

The CIS wave function is parameterized by the CIS amplitudes and MO coefficients, out of which only the CIS amplitudes are determined variationally. Therefore, the expectation value of  $\hat{\mu}_k\hat{\mu}_l$  over  $|\Psi_{\text{CIS}}\rangle$  will not equal the value obtained with the Hellmann–Feynman theorem. In such cases, the Hellmann–Feynman approach is preferred to taking the expectation value of the perturbing operator over the approximate wave function. Thus, the excited-state property for the operator  $\hat{\mu}_k\hat{\mu}_l$  is obtained by the Hellmann–Feynman method introduced in Eq. (17). The first step is to rewrite the CIS energy as

$$E_{\text{CIS}} = E_{\text{RHF}} + \Delta E_{\text{CIS}} = E_{\text{RHF}} + \sum_{ij}^{\text{occ}} \sum_{ab}^{\text{virt}} H_{ia,jb} c_{ia} c_{jb} \quad (21)$$

using Eq. (19). According to Eq. (17), we need to evaluate the derivative of the CIS energy

$$\left. \frac{dE_{\text{CIS}}(\lambda)}{d\lambda} \right|_{\lambda=0} = \left. \frac{dE_{\text{RHF}}(\lambda)}{d\lambda} \right|_{\lambda=0} + \left. \frac{d\Delta E_{\text{CIS}}(\lambda)}{d\lambda} \right|_{\lambda=0} \quad (22)$$

with respect to the perturbation parameter  $\lambda$  at  $\lambda = 0$ . In order to be consistent with the notation  $|\Phi_{i\sigma}^{a\sigma}\rangle$  used for singly-excited Slater determinants, we denote the ground-state RHF wave function as  $|\Phi_0\rangle$ . Since for the RHF method all wave function parameters (MO coefficients) are optimized by the variational principle, the derivative of the RHF energy is equal to the expectation value of  $\hat{\mu}_k\hat{\mu}_l$  over  $|\Phi_0\rangle$ , that is,

$$\left. \frac{dE_{\text{RHF}}(\lambda)}{d\lambda} \right|_{\lambda=0} = \langle \Phi_0 | \hat{\mu}_k \hat{\mu}_l | \Phi_0 \rangle \quad (23)$$

which can be evaluated using Eq. (15). The derivative of the CIS excitation energy reads

$$\left. \frac{d\Delta E_{\text{CIS}}(\lambda)}{d\lambda} \right|_{\lambda=0} = \sum_{ij}^{\text{occ}} \sum_{ab}^{\text{virt}} \left. \frac{dH_{ia,jb}(\lambda)}{d\lambda} \right|_{\lambda=0} c_{ia} c_{jb}. \quad (24)$$

Since the CIS amplitudes  $c_{ia}$  diagonalize the CIS Hamiltonian, their derivatives do not appear in Eq. (24). According to Eq. (18), matrix elements  $H_{ia,jb}$  depend on the MO energies and

MOs. Therefore, one has to take the derivative of the MO energies and MOs with respect to  $\lambda$ , which has been accomplished by solving the coupled-perturbed Hartree–Fock (CPHF) equations.<sup>112</sup> A more efficient method to evaluate CIS energy derivatives is based on the Lagrangian formalism for non-variational wave function parameters.<sup>109</sup>

As the excited state is obtained at the CIS level of theory, we choose to work with the RHF ground state  $|\Phi_0\rangle$  for the sake of consistency. Therefore, transition matrix elements of  $\hat{\mu}_k\hat{\mu}_l$  are to be computed between  $|\Phi_0\rangle$  and the lowest singlet CIS excited state  $|\Psi_{\text{CIS}}\rangle$ . This can be readily achieved by using the CIS expansion of Eq. (20), that is,

$$\langle\Phi_0|\hat{\mu}_k\hat{\mu}_l|\Psi_{\text{CIS}}\rangle = \frac{1}{\sqrt{2}} \sum_i^{\text{occ}} \sum_a^{\text{virt}} c_{ia} \left( \langle\Phi_0|\hat{\mu}_k\hat{\mu}_l|\Phi_{i\uparrow}^{a\uparrow}\rangle + \langle\Phi_0|\hat{\mu}_k\hat{\mu}_l|\Phi_{i\downarrow}^{a\downarrow}\rangle \right) \quad (25)$$

where matrix elements between the RHF reference and singly-excited Slater determinants can be evaluated by the Slater–Condon rules.<sup>109</sup>

### 3 Computational details

First, a brief description of the computational model is provided for the four-atomic formaldehyde ( $\text{H}_2\text{CO}$ ) molecule. Two singlet electronic states ( $S_0$  ( $\tilde{X}^1A_1$ ) and  $S_1$  ( $\tilde{A}^1A_2$ )) and two vibrational modes ( $\nu_2$  (C=O stretch) and  $\nu_4$  (out-of-plane)) are considered (2D( $\nu_2,\nu_4$ ) vibrational model, see Refs. 84–87,92,93 for further details). In addition, the orientation of the molecule is fixed with respect to the cavity polarization vector  $\vec{e}$ . The reference structure of  $\text{H}_2\text{CO}$  ( $C_{2v}$  point group symmetry) is shown in Fig. 1 where the definition of body-fixed Cartesian axes is also given. For the 2D( $\nu_2,\nu_4$ ) model, electronic structure computations were carried out at the DFT/TDDFT (CAM-B3LYP/6-31G\*) level of theory on a two-dimensional grid along the  $\nu_2$  and  $\nu_4$  vibrational modes, yielding ground-state (X) and excited-state (A) PESs, as well as permanent (PDM) and transition (TDM) dipole moment surfaces.

The electronic structure data are now supplemented by matrix elements of the operators  $\hat{\mu}_k\hat{\mu}_l$  in the basis of electronic states. As these quantities are not available in standard elec-

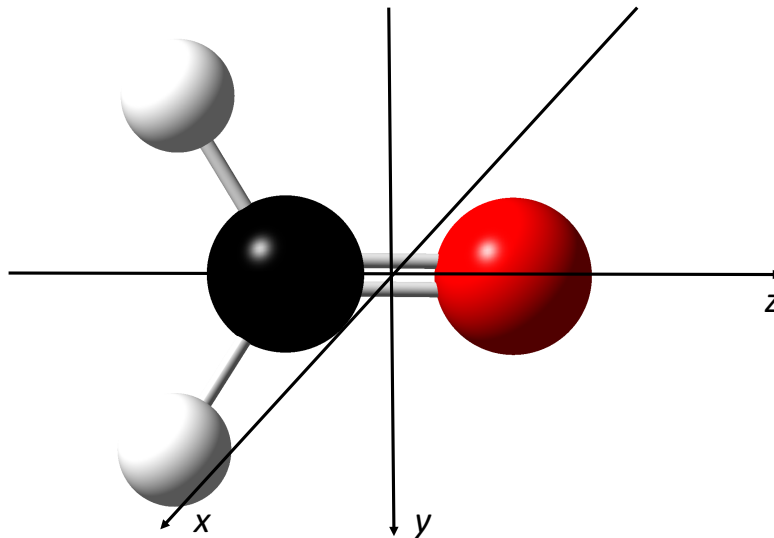


Figure 1: Reference structure of formaldehyde ( $\text{H}_2\text{CO}$ ,  $C_{2v}$  point group symmetry) and definition of body-fixed Cartesian axes. The planar reference structure is placed in the  $yz$  plane.

tronic structure packages, we propose an easy-to-implement yet sensible approach based on wave-function methods. The ground-state expectation value of  $\hat{\mu}_k \hat{\mu}_l$  is evaluated using Eqs. (13), (14) and (15) at the RHF (restricted Hartree–Fock) level of theory. The excited state considered by the current work is the lowest singlet excited state of  $\text{H}_2\text{CO}$ , corresponding to a HOMO-LUMO excitation. Thus, we have to deal with an open-shell singlet state which cannot be described by a single Slater determinant. Therefore, the configuration interaction singles (CIS) method is invoked to obtain the excited state. The excited-state property for  $\hat{\mu}_k \hat{\mu}_l$  and the matrix element  $\langle X | \hat{\mu}_k \hat{\mu}_l | A \rangle$  are evaluated by Eqs. (17) and (25), respectively. In all computations, we have used the 6-31G\* basis set. The necessary integrals, canonical molecular orbitals, orbital energies and RHF reduced density matrices have been computed with the PySCF ab initio program package.<sup>113,114</sup> The methodology based on the RHF and CIS levels of theory has been validated by comparing several RHF/6-31G\* and CIS/6-31G\* quantities (excitation energies, PDM and TDM values) to their DFT and TDDFT (CAM-B3LYP/6-31G\*) counterparts. The RHF/CIS and DFT/TDDFT methods have been found to give good agreement for all quantities considered.

At the reference structure, the X and A electronic states transform according to the irreducible representations (irreps)  $\Gamma_X = A_1$  and  $\Gamma_A = A_2$  of the  $C_{2v}$  point group, respectively, while the two vibrational modes are of  $\Gamma_{\nu_2} = A_1$  and  $\Gamma_{\nu_4} = B_1$  symmetries. In addition, the body-fixed Cartesian coordinates transform according to the irreps  $\Gamma_x = B_1$ ,  $\Gamma_y = B_2$  and  $\Gamma_z = A_1$ . Table 1 provides a detailed symmetry analysis for electronic matrix elements of the operators  $\hat{\mu}_k$  and  $\hat{\mu}_k\hat{\mu}_l$ . These matrix elements can have nonvanishing values at the reference geometry only in case of the  $A_1$  irrep. Moreover, for the  $B_1$  irrep, although matrix elements of  $\hat{\mu}_k$  and  $\hat{\mu}_k\hat{\mu}_l$  are zero at the reference geometry, one can produce nonzero matrix elements by displacement from the reference structure along the  $\nu_4$  vibrational mode of  $B_1$  symmetry.

Table 1: Symmetry properties (irreducible representations of the  $C_{2v}$  point group) of electronic matrix elements ( $\langle\alpha|\hat{O}|\alpha\rangle$  with  $\alpha = X, A$  and  $\langle X|\hat{O}|A\rangle$ ) for the operators  $\hat{O} = \hat{\mu}_k$  and  $\hat{O} = \hat{\mu}_k\hat{\mu}_l$  ( $k, l = x, y, z$ ). See Eqs. (10) and (11) for the definition of  $\hat{\mu}_k$  and  $\hat{\mu}_k\hat{\mu}_l$ . Note that  $\Gamma_X = A_1$ ,  $\Gamma_A = A_2$ ,  $\Gamma_x = B_1$ ,  $\Gamma_y = B_2$  and  $\Gamma_z = A_1$ .

operator ( $\hat{O}$ )	symmetry for $\langle\alpha \hat{O} \alpha\rangle$ ( $\alpha = X, A$ )	symmetry for $\langle X \hat{O} A\rangle$
$\hat{\mu}_x$	$\Gamma_\alpha \otimes \Gamma_x \otimes \Gamma_\alpha = B_1$	$\Gamma_X \otimes \Gamma_x \otimes \Gamma_A = B_2$
$\hat{\mu}_y$	$\Gamma_\alpha \otimes \Gamma_y \otimes \Gamma_\alpha = B_2$	$\Gamma_X \otimes \Gamma_y \otimes \Gamma_A = B_1$
$\hat{\mu}_z$	$\Gamma_\alpha \otimes \Gamma_z \otimes \Gamma_\alpha = A_1$	$\Gamma_X \otimes \Gamma_z \otimes \Gamma_A = A_2$
$\hat{\mu}_x^2$	$\Gamma_\alpha \otimes \Gamma_x \otimes \Gamma_x \otimes \Gamma_\alpha = A_1$	$\Gamma_X \otimes \Gamma_x \otimes \Gamma_x \otimes \Gamma_A = A_2$
$\hat{\mu}_y^2$	$\Gamma_\alpha \otimes \Gamma_y \otimes \Gamma_y \otimes \Gamma_\alpha = A_1$	$\Gamma_X \otimes \Gamma_y \otimes \Gamma_y \otimes \Gamma_A = A_2$
$\hat{\mu}_z^2$	$\Gamma_\alpha \otimes \Gamma_z \otimes \Gamma_z \otimes \Gamma_\alpha = A_1$	$\Gamma_X \otimes \Gamma_z \otimes \Gamma_z \otimes \Gamma_A = A_2$
$\hat{\mu}_x\hat{\mu}_y$	$\Gamma_\alpha \otimes \Gamma_x \otimes \Gamma_y \otimes \Gamma_\alpha = A_2$	$\Gamma_X \otimes \Gamma_x \otimes \Gamma_y \otimes \Gamma_A = A_1$
$\hat{\mu}_x\hat{\mu}_z$	$\Gamma_\alpha \otimes \Gamma_x \otimes \Gamma_z \otimes \Gamma_\alpha = B_1$	$\Gamma_X \otimes \Gamma_x \otimes \Gamma_z \otimes \Gamma_A = B_2$
$\hat{\mu}_y\hat{\mu}_z$	$\Gamma_\alpha \otimes \Gamma_y \otimes \Gamma_z \otimes \Gamma_\alpha = B_2$	$\Gamma_X \otimes \Gamma_y \otimes \Gamma_z \otimes \Gamma_A = B_1$

In all quantum-dynamical computations, the wave function of the coupled cavity-molecule system has been represented in the basis  $|\alpha in\rangle$  where  $\alpha = X, A$  labels molecular electronic states,  $i$  denotes two-dimensional direct-product Fourier discrete variable representation (DVR)<sup>115</sup> basis functions (used for the  $\nu_2$  and  $\nu_4$  vibrational modes) and  $n = 0, 1, 2, 3$  ( $n$  labels Fock states of the cavity mode). Normal coordinates ( $Q_2$  and  $Q_4$ ) are used and the kinetic energy operator is equal to  $\hat{T} = -\frac{\hbar^2}{2} \left( \frac{\partial^2}{\partial Q_2^2} + \frac{\partial^2}{\partial Q_4^2} \right)$ . 37 and 51 equidistant Fourier DVR points have been applied in the intervals  $[-110\sqrt{m_e}a_0, 70\sqrt{m_e}a_0]$  and

$[-125\sqrt{m_e a_0}, 125\sqrt{m_e a_0}]$  for  $Q_2$  and  $Q_4$ , respectively. The dimension of the two-dimensional direct-product DVR basis equals  $37 \cdot 51 = 1887$ . Time propagation of the wave function has been carried out with the explicit third-order Adams–Bashforth method<sup>116</sup> with a time step of 0.005 fs and the norm of the wave function has been set to one at each step of the time propagation. As discussed in Section 2, the molecule is coupled to a single quantized mode of an optical cavity. Then, the molecule is pumped with a laser pulse which couples the electronic states X and A. Since in the  $2D(\nu_2, \nu_4)$  model the X and A PDMs are perpendicular to the TDM and the polarization vector of the laser field is chosen parallel to the TDM, the pump pulse interacts only with the TDM of the molecule.

## 4 Results and discussion

Having described the theoretical details and computational models, we will now examine electronic structure and quantum-dynamical results. We consider single-molecule strong coupling conditions which imply that the ground (lowest) polaritonic state essentially equals  $|X0\rangle$  (electronic ground state with zero photons), while the lower (1LP) and upper (1UP) polaritonic states can be well approximated as the linear combinations of  $|X1\rangle$  and  $|A0\rangle$  (singly-excited subspace). Similarly, higher-lying polaritonic states can be denoted as  $n$ LP and  $n$ UP (with  $n > 1$ ). As already outlined in Section 3, our computations are numerically exact including all cavity-molecule coupling terms and the nomenclature is only used to guide the discussion.

After summarizing the electronic structure results relevant for the DSE term, we will discuss the impact of DSE on the light-induced conical intersection (LICI) and the ensuing cavity-induced nonadiabatic effects. Thereby, time-dependent quantum-dynamical results with and without the inclusion of the DSE term in the cavity-molecule Hamiltonian will be presented and compared. To this end, the system is prepared in an initial state which corresponds to the ground state of the coupled cavity-molecule system. Then, the system

is excited by a pump laser pulse which transfers population primarily to the 1LP and 1UP polaritonic states. Time-dependent populations of the 1LP and 1UP states will highlight the impact of the DSE term.

## 4.1 Electronic structure results

This subsection discusses electronic structure results relevant for the DSE term. Namely, ground-state and excited-state electronic matrix elements of the operators  $\hat{\mu}_k\hat{\mu}_l$  as well as transition matrix elements  $\langle X|\hat{\mu}_k\hat{\mu}_l|A\rangle$  are presented. Due to the high symmetry of the molecule, many matrix elements vanish and in Figs. 2, 3 and 4, all nonzero  $\hat{\mu}_k\hat{\mu}_l$  matrix elements are shown. Note that numerical results (i.e., which  $\hat{\mu}_k\hat{\mu}_l$  operators yield nonzero matrix elements) are in line with group-theoretical considerations described in Section 3 and Table 1. Figs. 2 and 3 compare the ground-state (RHF/6-31G\*) and excited-state (CIS/6-31G\*) matrix elements of the operators  $\hat{\mu}_k\hat{\mu}_l$  for one-dimensional scans along the  $\nu_2$  and  $\nu_4$  vibrational modes, respectively. In each case, rectilinear normal coordinates ( $Q_2$  and  $Q_4$ ) are used and the inactive normal coordinate is set to zero. It is visible in Fig. 3 that the only nonzero offdiagonal matrix element ( $\hat{\mu}_x\hat{\mu}_z$ ) vanishes for  $Q_4 = 0$  and its value is smaller than those of the diagonal components  $\hat{\mu}_k^2$  by an order of magnitude. In addition, Fig. 4 presents nonzero transition matrix elements of  $\hat{\mu}_x\hat{\mu}_y$  and  $\hat{\mu}_y\hat{\mu}_z$  between the ground and excited electronic states, again along the  $\nu_2$  and  $\nu_4$  modes. In this case, all diagonal components  $\hat{\mu}_k^2$  yield zero transition matrix elements. Furthermore, the magnitudes of transition matrix elements shown in Fig. 4 are considerably smaller than those of the ground-state and excited-state matrix elements of the diagonal components  $\hat{\mu}_k^2$  (see Figs. 2 and 3).

## 4.2 Light-induced nonadiabatic effects

This subsection provides a discussion of how and to what extent LICIs are affected by the DSE. We set the cavity polarization to  $\mathbf{e} = (1, 1, 1)/\sqrt{3}$  which assures that all nonzero TDM,

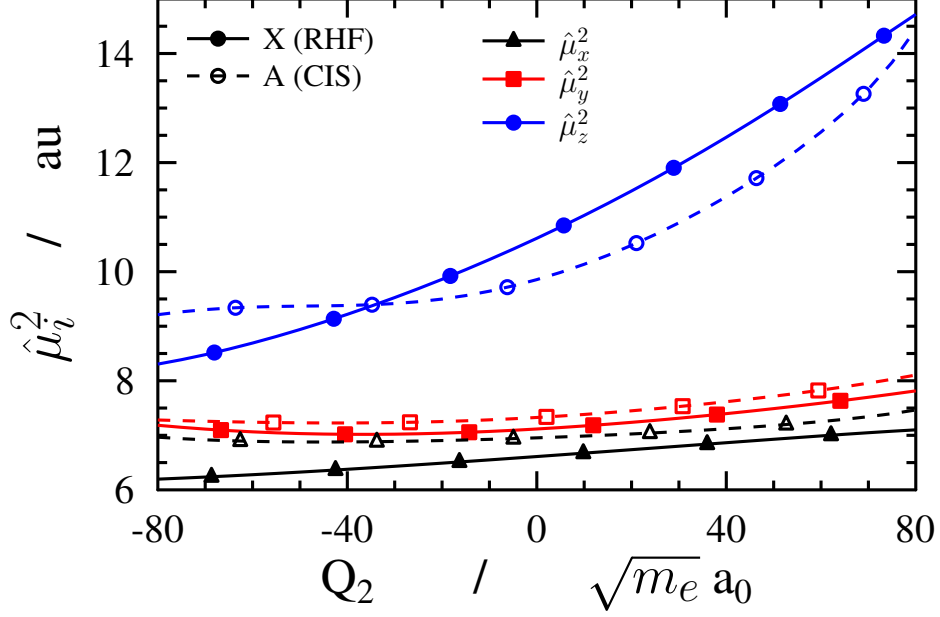


Figure 2: Ground-state (X) and excited-state (A) electronic matrix elements of  $\hat{\mu}_x^2$ ,  $\hat{\mu}_y^2$  and  $\hat{\mu}_z^2$  in atomic units, obtained at the RHF/6-31G\* (X) and CIS/6-31G\* (A) levels of theory along the  $\nu_2$  (C=O stretch) normal mode. All other  $\hat{\mu}_k\hat{\mu}_l$  matrix elements are zero (see Table 1).

PDM and DSE terms come into play. Namely, in the 2D( $\nu_2, \nu_4$ ) model, we get

$$\langle \alpha | \hat{\mu} \vec{e} | \alpha \rangle = \frac{1}{\sqrt{3}} \sum_{k=x,z} \langle \alpha | \hat{\mu}_k | \alpha \rangle \quad (26)$$

and

$$\langle X | \hat{\mu} \vec{e} | A \rangle = \frac{1}{\sqrt{3}} \langle X | \hat{\mu}_y | A \rangle \quad (27)$$

where  $\alpha = X, A$  labels electronic states and the group-theoretical results of Table 1 can be used to assess that the  $y$  component of the PDMs and the  $x$  and  $z$  components of the TDM vanish due to symmetry. Similarly, for the DSE, one can show that

$$\langle \alpha | (\hat{\mu} \vec{e})^2 | \alpha \rangle = \frac{1}{3} \sum_{k=x,y,z} \langle \alpha | \hat{\mu}_k^2 | \alpha \rangle + \frac{2}{3} \langle \alpha | \hat{\mu}_x \hat{\mu}_z | \alpha \rangle \quad (28)$$

and

$$\langle X | (\hat{\mu} \vec{e})^2 | A \rangle = \frac{2}{3} (\langle X | \hat{\mu}_x \hat{\mu}_y | A \rangle + \langle X | \hat{\mu}_y \hat{\mu}_z | A \rangle). \quad (29)$$

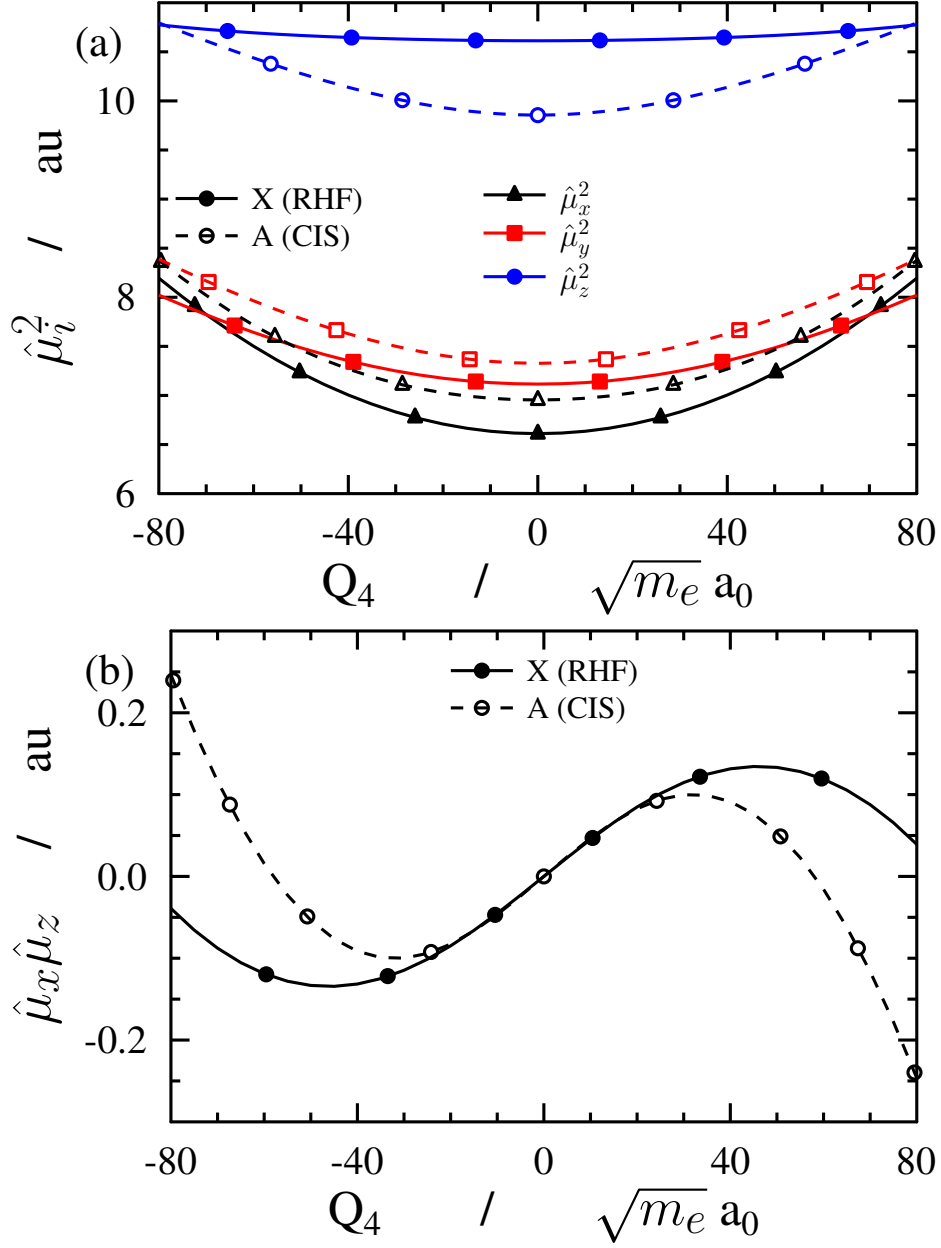


Figure 3: Ground-state (X) and excited-state (A) electronic matrix elements of  $\hat{\mu}_x^2$ ,  $\hat{\mu}_y^2$  and  $\hat{\mu}_z^2$  (panel a), and  $\hat{\mu}_x \hat{\mu}_z$  (panel b) in atomic units, obtained at the RHF/6-31G\* (X) and CIS/6-31G\* (A) levels of theory along the  $\nu_4$  (out-of-plane) normal mode. All other  $\hat{\mu}_k \hat{\mu}_l$  matrix elements are zero (see Table 1).

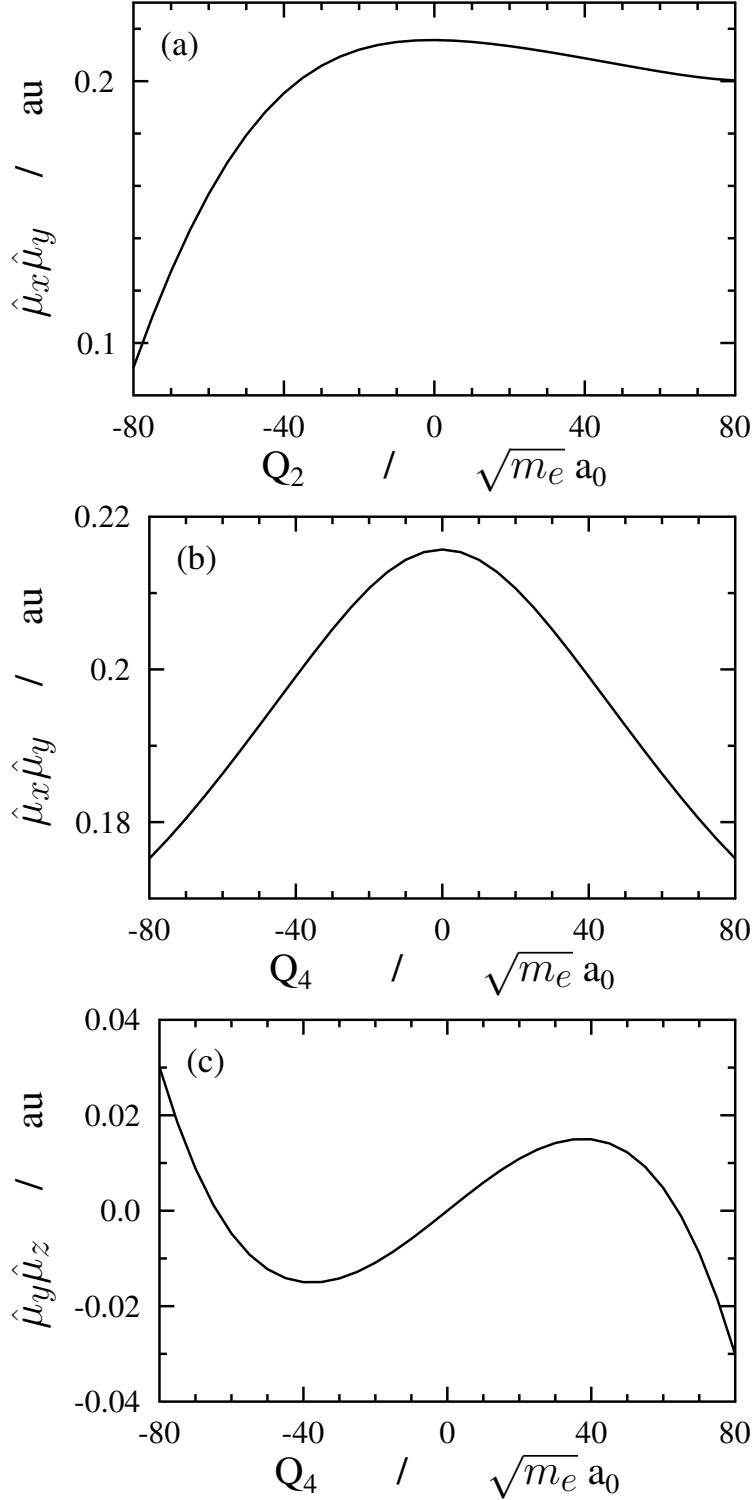


Figure 4: Electronic transition matrix elements of the operators  $\hat{\mu}_x \hat{\mu}_y$  and  $\hat{\mu}_y \hat{\mu}_z$  between the ground (X) and excited (A) electronic states in atomic units, obtained at the RHF/6-31G\* (X) and CIS/6-31G\* (A) levels of theory (panels a and b:  $\langle X | \hat{\mu}_x \hat{\mu}_y | A \rangle$  along the  $\nu_2$  (C=O stretch) and  $\nu_4$  (out-of-plane) normal modes, panel c:  $\langle X | \hat{\mu}_y \hat{\mu}_z | A \rangle$  along the  $\nu_4$  normal mode.) Note that all nonvanishing transition matrix elements are shown (see Table 1).

One-dimensional scans for  $\langle \alpha | (\hat{\mu}\vec{e})^2 | \alpha \rangle$  and  $\langle X | (\hat{\mu}\vec{e})^2 | A \rangle$  along the  $\nu_2$  and  $\nu_4$  normal modes are shown in Fig. 5.

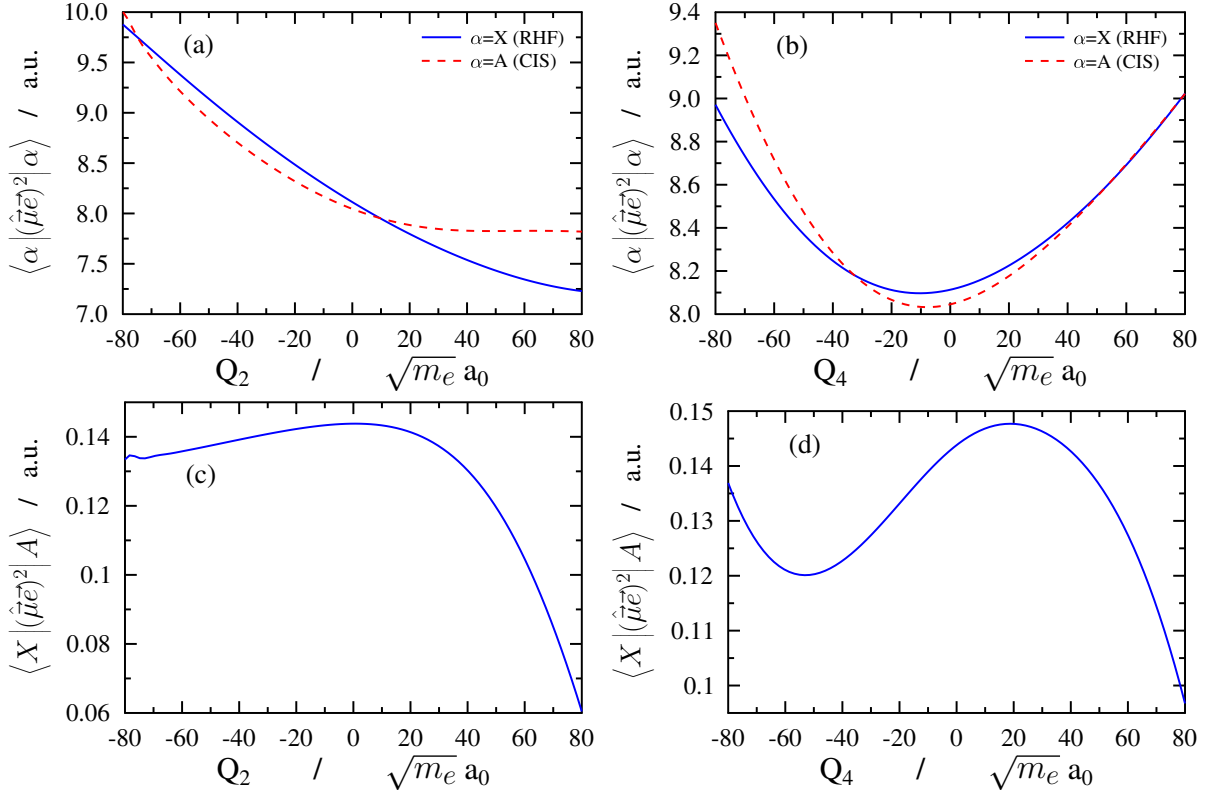


Figure 5: Ground-state (X) and excited-state (A) electronic matrix elements  $\langle \alpha | (\hat{\mu}\vec{e})^2 | \alpha \rangle$  ( $\alpha = X, A$ ) in atomic units, obtained at the RHF/6-31G\* (X) and CIS/6-31G\* (A) levels of theory along the  $\nu_2$  (C=O stretch, panel a) and  $\nu_4$  (out-of-plane, panel b) normal modes. Electronic transition matrix elements  $\langle X | (\hat{\mu}\vec{e})^2 | A \rangle$  are also shown in atomic units along the  $\nu_2$  (panel c) and  $\nu_4$  (panel d) normal modes. In all cases, the polarization vector is chosen as  $\mathbf{e} = (1, 1, 1)/\sqrt{3}$ .  $Q_2$  and  $Q_4$  denote normal coordinates of the  $\nu_2$  and  $\nu_4$  normal modes, respectively. Note that curves along  $Q_4$  (panels b and d) are neither symmetric, nor anti-symmetric under the transformation  $Q_4 \rightarrow -Q_4$ .

Polaritonic PESs can be constructed by diagonalizing the potential energy part of the cavity-molecule Hamiltonian of Eq. (2), either with or without the DSE term. Fig. 6 shows the 1LP and 1UP polaritonic PESs for  $\omega_c = 34304.93 \text{ cm}^{-1}$ ,  $g = 0.01 \text{ au}$  and  $\mathbf{e} = (1, 1, 1)/\sqrt{3}$  with the DSE included in the potential energy matrix. We note that  $g$  has the dimension of electric field and the coupling energy can be given as the product of  $g$  and the molecular dipole moment. Since the TDM varies between  $-0.2 \text{ au}$  and  $0.2 \text{ au}$  in the nuclear configuration

space relevant for the current results, the coupling energy between electronic states X and A does not exceed  $\sim 500 \text{ cm}^{-1}$ . It is visible in Fig. 6 that the 1LP and 1UP PES form a LICI, which is also the case if the DSE is omitted from the potential energy matrix. However, the DSE modifies the position of the LICI. Namely, without DSE, the LICI is situated at  $Q_2 = 27.4745\sqrt{m_e}a_0$  and  $Q_4 = 0$ , which is shifted to  $Q_2 = 27.3724\sqrt{m_e}a_0$  and  $Q_4 = 0.0179\sqrt{m_e}a_0$  if the DSE is taken into account. The energetic position of the LICI corresponds to  $34826.86 \text{ cm}^{-1}$  without DSE and  $34797.91 \text{ cm}^{-1}$  with DSE, both referenced to the minimum of the respective ground (lowest) polaritonic PES. LICI positions are explicitly marked in Fig. 7 where differences between polaritonic PESs obtained with and without the DSE term are shown for the 1LP and 1UP polaritonic states.

Although  $V_X(Q_2, -Q_4) = V_X(Q_2, Q_4)$  and  $V_A(Q_2, -Q_4) = V_A(Q_2, Q_4)$ , the “difference polaritonic” PESs in Fig. 7 are not symmetric under the transformation  $Q_4 \rightarrow -Q_4$ . The same observation applies to the polaritonic PESs themselves, which can be understood by inspecting the symmetry of the TDM, PDM and DSE terms. Using the data given in Table 1, one can determine that the  $z$  component of the PDM is symmetric while the  $x$  component of the PDM and the  $y$  component of the TDM are antisymmetric under  $Q_4 \rightarrow -Q_4$ . Therefore, the expression for  $\langle \alpha | \hat{\mu} \vec{e} | \alpha \rangle$  in Eq. (26) is neither symmetric nor antisymmetric, which breaks the symmetry of the resulting polaritonic PESs. However, if the DSE is omitted, the LICI is still located at a symmetric position with  $Q_4 = 0$ . The DSE terms in Eqs. (28) and (29) induce further symmetry breaking, which is also visible in panels b and d of Fig. 5 (that is, one-dimensional  $\langle \alpha | (\hat{\mu} \vec{e})^2 | \alpha \rangle$  and  $\langle X | (\hat{\mu} \vec{e})^2 | A \rangle$  curves as a function of  $Q_4$  are neither symmetric, nor antisymmetric under  $Q_4 \rightarrow -Q_4$ ). As a consequence, the position of the LICI is shifted to  $Q_4 \neq 0$  if the DSE is included in the potential energy matrix.

### 4.3 Time-dependent quantum dynamics

In this subsection, differences between time-dependent quantum-dynamical results obtained with and without the DSE term are discussed. Two different cavity wavenumber values of

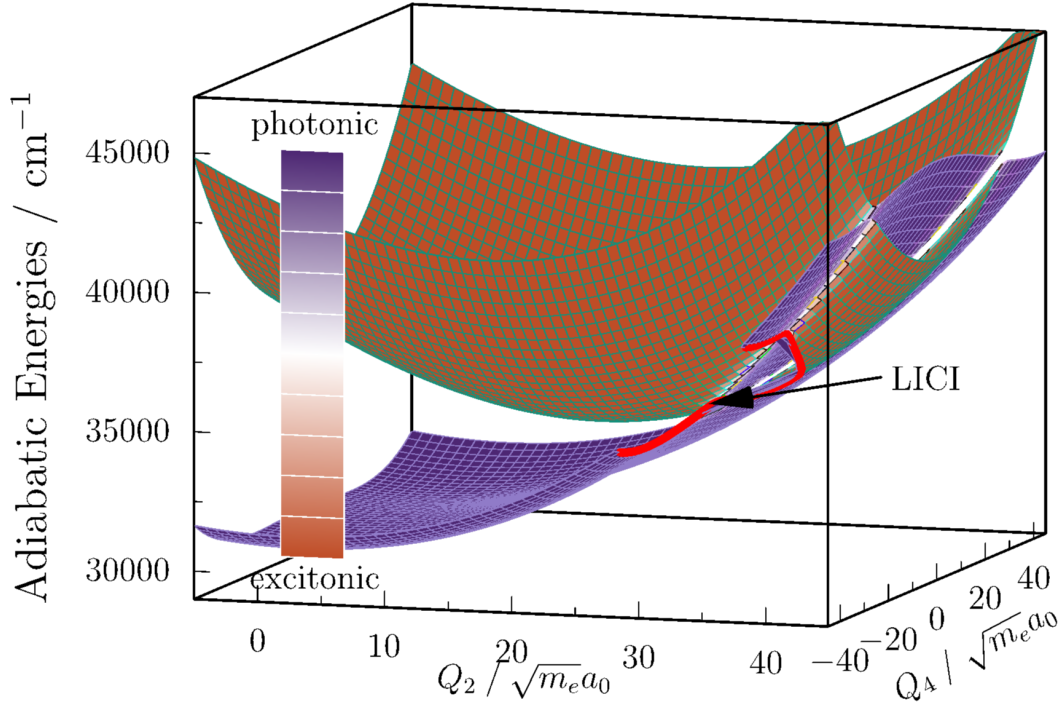


Figure 6: Two-dimensional lower (1LP) and upper (1UP) polaritonic potential energy surfaces (PESs), including the dipole self-energy term.  $Q_2$  and  $Q_4$  denote normal coordinates of the  $\nu_2$  (C=O stretch) and  $\nu_4$  (out-of-plane) normal modes. The cavity wavenumber, coupling strength and polarization are chosen as  $\omega_c = 34304.93 \text{ cm}^{-1}$ ,  $g = 0.01 \text{ au}$  and  $\mathbf{e} = (1, 1, 1)/\sqrt{3}$ , respectively. The character of the polaritonic PESs is indicated by different colors (purple: photonic, orange: excitonic). The light-induced conical intersection (LICI, located at  $Q_2 = 27.3724\sqrt{m_e a_0}$  and  $Q_4 = 0.0179\sqrt{m_e a_0}$ ) between the 1LP and 1UP PESs is explicitly marked in the figure. Polaritonic PESs are referenced to the minimum of the ground (lowest) polaritonic PES. A half circle (shown in red) is cut from the 1LP PES in order to make the LICI visible.

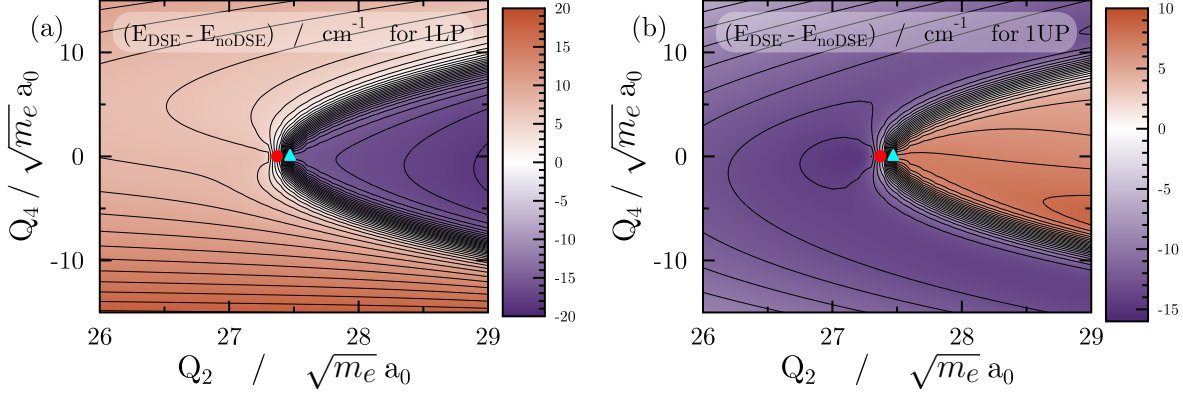


Figure 7: Differences between polaritonic potential energy surfaces (PESs) obtained with and without the dipole self-energy (DSE) term for the 1LP (panel a) and 1UP (panel b) polaritonic states.  $Q_2$  and  $Q_4$  denote normal coordinates of the  $\nu_2$  (C=O stretch) and  $\nu_4$  (out-of-plane) normal modes. The cavity wavenumber, coupling strength and polarization are chosen as  $\omega_c = 34304.93 \text{ cm}^{-1}$ ,  $g = 0.01 \text{ au}$  and  $\mathbf{e} = (1, 1, 1)/\sqrt{3}$ , respectively. Positions of the light-induced conical intersection between the 1LP and 1UP polaritonic PESs are explicitly marked by the symbols  $\blacktriangle$  (without DSE,  $Q_2 = 27.4745\sqrt{m_e}a_0$  and  $Q_4 = 0$ ) and  $\bullet$  (with DSE,  $Q_2 = 27.3724\sqrt{m_e}a_0$  and  $Q_4 = 0.0179\sqrt{m_e}a_0$ ). Polaritonic PESs are referenced to the minimum of the ground (lowest) polaritonic PES.

$\omega_c = 34304.93 \text{ cm}^{-1}$  and  $\omega_c = 34370.27 \text{ cm}^{-1}$  are employed, while the other cavity parameters are set to  $g = 0.01 \text{ au}$ ,  $\gamma_c = 10^{-4} \text{ au}$  (equivalent to a lifetime of  $\tau = \hbar/\gamma_c = 241.9 \text{ fs}$ ) and  $\mathbf{e} = (1, 1, 1)/\sqrt{3}$ . The molecule coupled to a single cavity mode is pumped with a laser pulse, the laser intensity equals  $I = 5 \text{ TW/cm}^2$  and the pulse length is chosen as  $T = 200 \text{ fs}$  (see the text under Eq. (5) for the definition of the envelope function). The field amplitude  $E_0$  is related to the intensity by the formula  $E_0 = \sqrt{2I/(c\epsilon_0)}$  ( $c$  is the speed of light in vacuum and  $\epsilon_0$  is the vacuum permittivity).

First, the laser wavenumber is set to  $\omega = 34300 \text{ cm}^{-1}$ . Fig. 8 shows time-dependent populations of the 1LP and 1UP polaritonic states during and after laser excitation. Panels a and c, and panels b and d present results with and without the DSE term, respectively. Data depicted in panels a and b of Fig. 8 were obtained with  $\omega_c = 34304.93 \text{ cm}^{-1}$ , while panels c and d correspond to  $\omega_c = 34370.27 \text{ cm}^{-1}$  (these choices for  $\omega_c$  will be justified later). It is easy to notice the similarity between panels a and d, and panels b and c of Fig. 8. In addition, even though the DSE adds relatively small shifts to the energy levels and potentials,

panels of Fig. 8 also show how sensitive the dynamics is to the value of  $\omega_c$  and whether the DSE is included in the cavity-molecule Hamiltonian. Similar conclusions can be drawn by inspecting Fig. 9 (following the structure of Fig. 8) where populations of cavity-molecule eigenstates relevant for the dynamics are shown between 0 fs and  $T = 200$  fs. If the DSE term is taken into account and  $\omega_c = 34304.93 \text{ cm}^{-1}$ , dominantly one eigenstate ( $34391.28 \text{ cm}^{-1}$ , referenced to the lowest energy level of  $1526.94 \text{ cm}^{-1}$ , see panel a) is populated by the laser pulse, while without the DSE the population is mainly transferred to two close-lying eigenstates ( $34290.73 \text{ cm}^{-1}$  and  $34335.73 \text{ cm}^{-1}$ , both referenced to the lowest energy level of  $1522.71 \text{ cm}^{-1}$ , see panel b) with  $\omega_c = 34304.93 \text{ cm}^{-1}$ . The latter two eigenstates can be characterized as superpositions of the X vibrational ground state ( $1521.48 \text{ cm}^{-1}$ , dressed with one photon) and an excited A vibrational eigenstate ( $35826.42 \text{ cm}^{-1}$ , dressed with zero photons) which are resonantly coupled by the cavity mode. If the DSE term is included in the Hamiltonian, the cavity frequency is no longer resonant with any of the X  $\rightarrow$  A transitions and the dominantly-populated cavity-molecule eigenstate can be well approximated as an A vibrational eigenstate with zero photons.

If the DSE is taken into account, the Hamiltonians

$$\hat{H}_\alpha = \hat{T} + \hat{V}_\alpha + \frac{g^2}{\hbar\omega_c} \hat{D}_\alpha \quad (30)$$

appearing on the diagonal of the matrix Hamiltonian of Eq. (2) are central to determining conditions for resonant cavity-molecule coupling. Here,  $\hat{D}_\alpha = \langle \alpha | (\vec{\mu}\vec{e})^2 | \alpha \rangle$  with  $\alpha = \text{X, A}$ , and the ground-state and excited-state PESs are shifted by the DSE terms proportional to  $\hat{D}_\alpha$ . As a consequence, the effective X and A vibrational energy levels become dependent on cavity parameters, which renders the condition for resonant cavity-molecule coupling less obvious than in the no DSE case where the resonance condition is that levels of X shifted by  $\hbar\omega_c$  coincide with levels of A. One can apply first-order perturbation theory to approximate

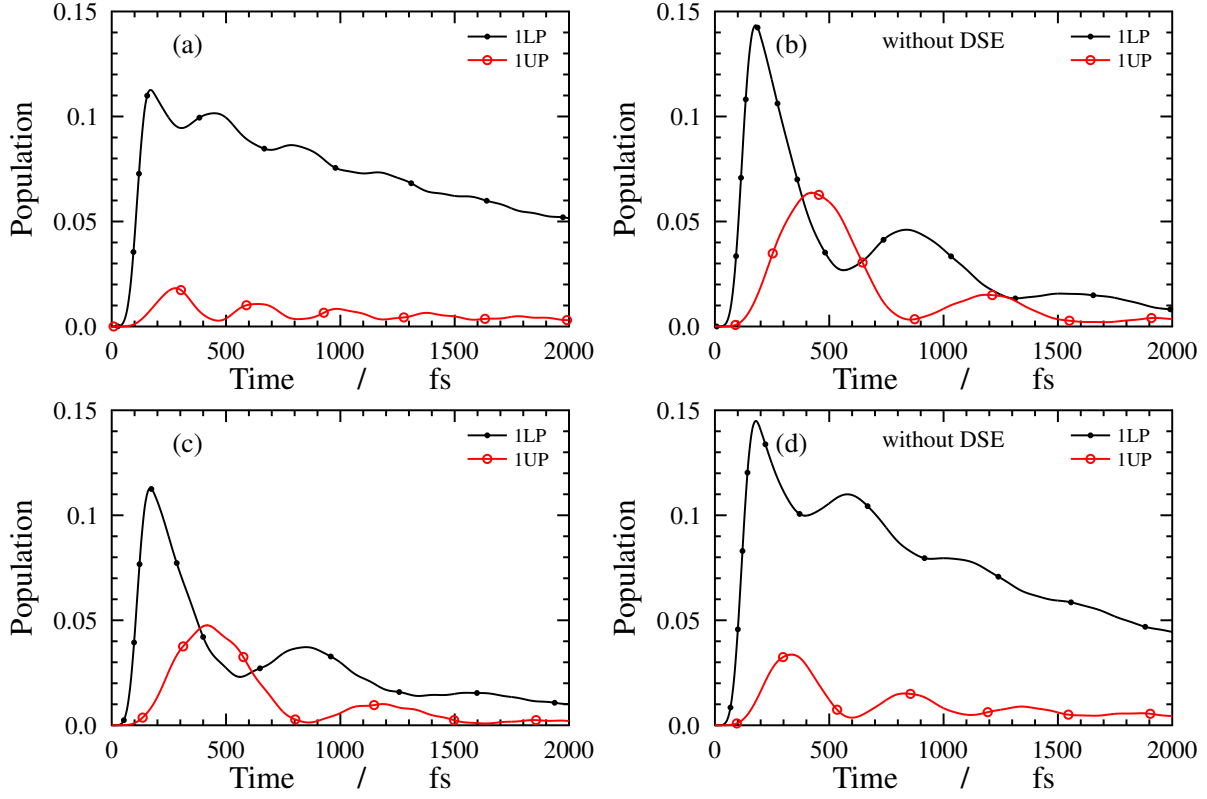


Figure 8: Populations of polaritonic states (1LP and 1UP) as a function of time obtained with (panels a and c) and without (panels b and d) the DSE term. The cavity wavenumber is chosen as  $\omega_c = 34304.93 \text{ cm}^{-1}$  (panels a and b) and  $\omega_c = 34370.27 \text{ cm}^{-1}$  (panels c and d). Other cavity and laser parameters equal  $g = 0.01 \text{ au}$ ,  $\gamma_c = 10^{-4} \text{ au}$ ,  $\mathbf{e} = (1, 1, 1)/\sqrt{3}$ ,  $\omega = 34300 \text{ cm}^{-1}$ ,  $I = 5 \text{ TW/cm}^2$  and  $T = 200 \text{ fs}$ . Note the sensitivity of 1LP and 1UP populations to  $\omega_c$  and the similarity between panels a and d, and panels b and c.

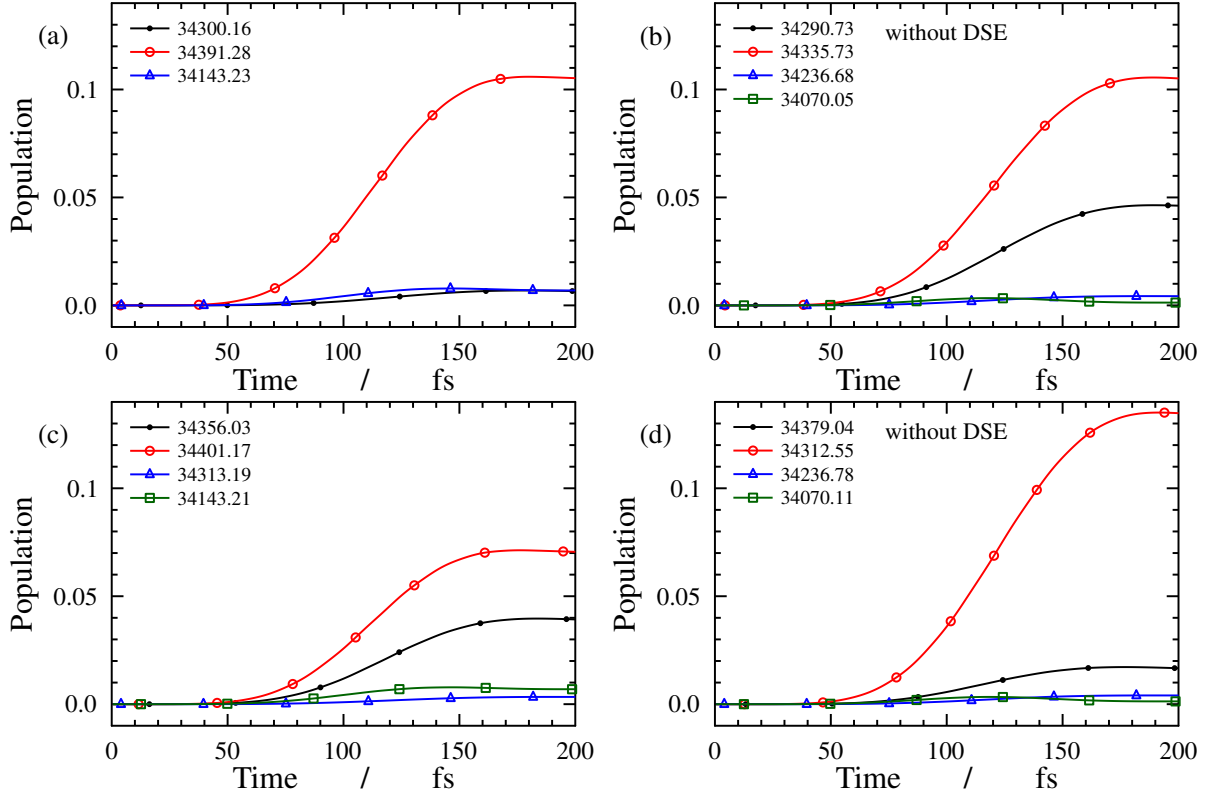


Figure 9: Populations of cavity-molecule eigenstates populated by laser excitation as a function of time (panels a and c: with DSE, panels b and d: without DSE). The cavity wavenumber is chosen as  $\omega_c = 34304.93 \text{ cm}^{-1}$  (panels a and b) and  $\omega_c = 34370.27 \text{ cm}^{-1}$  (panels c and d). Other cavity and laser parameters equal  $g = 0.01 \text{ au}$ ,  $\gamma_c = 10^{-4} \text{ au}$ ,  $\mathbf{e} = (1, 1, 1)/\sqrt{3}$ ,  $\omega = 34300 \text{ cm}^{-1}$ ,  $I = 5 \text{ TW/cm}^2$  and  $T = 200 \text{ fs}$ . Energy levels in the plot legends are given in units of  $\text{cm}^{-1}$  and referenced to the lowest energy level. Note the sensitivity of eigenstate populations to  $\omega_c$  and the similarity between panels a and d, and panels b and c.

the energy levels of  $\hat{H}_\alpha$ , which yields

$$E_{\alpha,i} = E_{\alpha,i}^{(0)} + \frac{g^2}{\hbar\omega_c} \langle \psi_{\alpha,i}^{(0)} | \hat{D}_\alpha | \psi_{\alpha,i}^{(0)} \rangle \quad (31)$$

where zeroth-order energy levels and eigenstates are defined in the absence of DSE by

$$\hat{H}_\alpha^{(0)} | \psi_{\alpha,i}^{(0)} \rangle = E_{\alpha,i}^{(0)} | \psi_{\alpha,i}^{(0)} \rangle \quad (32)$$

with  $\hat{H}_\alpha^{(0)} = \hat{T} + \hat{V}_\alpha$ . With this, the resonance condition can be readily formulated as

$$E_{A,j} - E_{X,i} = E_{A,j}^{(0)} - E_{X,i}^{(0)} + \frac{g^2}{\hbar\omega_c} (\langle \psi_{A,j}^{(0)} | \hat{D}_A | \psi_{A,j}^{(0)} \rangle - \langle \psi_{X,i}^{(0)} | \hat{D}_X | \psi_{X,i}^{(0)} \rangle) = \hbar\omega_c \quad (33)$$

which can be solved for the resonance frequency  $\omega_c$ .

Using Eq. (33) and choosing  $E_{A,j}^{(0)} = 35826.42 \text{ cm}^{-1}$  and  $E_{X,i}^{(0)} = 1521.48 \text{ cm}^{-1}$  (these are the vibrational levels that are resonantly coupled by the cavity for  $\omega_c = 34304.93 \text{ cm}^{-1}$  if the DSE is omitted), the resonant cavity wavenumber becomes  $\omega_c = 34370.27 \text{ cm}^{-1}$  for the DSE case. Panels c and d of Fig. 8 show 1LP and 1UP populations (panel c: with DSE, panel d: without DSE) for  $\omega_c = 34370.27 \text{ cm}^{-1}$ . Now, due to the modified cavity wavenumber, cavity-molecule resonance occurs if the DSE term is included and resonance is disrupted if the DSE is neglected. Populations of relevant cavity-molecule eigenstates shown in panels c and d of Fig. 9 further support the conclusions drawn here. The analysis of resonance conditions also clarifies why panels a and d, and panels b and c are similar to each other in Figs. 8 and 9. Namely, in both figures, panels a and d correspond to the nonresonant DSE and no DSE cases, while panels b and c pertain to resonant cavity-molecule coupling.

Figs. 10 and 11 depict 1LP and 1UP probability densities for cavity-molecule eigenstates relevant for the interpretation of the current results. It can be seen that one can establish a one-to-one correspondence between eigenstates obtained with and without the DSE term. Namely, Fig. 10 compares 1LP and 1UP probability densities for the eigenstates

34391.28  $\text{cm}^{-1}$  (with DSE) and 34312.55  $\text{cm}^{-1}$  (without DSE), both of which correspond to the dominantly-populated eigenstates in the nonresonant cases of Fig. 9. Moreover, Fig. 11 relates relevant eigenstates of the resonant DSE and no DSE cases (34401.17  $\text{cm}^{-1}$  with DSE and 34335.73  $\text{cm}^{-1}$  without DSE, 34356.03  $\text{cm}^{-1}$  with DSE and 34290.73  $\text{cm}^{-1}$  without DSE). For all eigenstate pairs, the respective probability densities agree well. It is also clear from the results that the DSE perturbs the relevant energy levels by less than 100  $\text{cm}^{-1}$  (when referenced to the lowest energy level) in this particular case.

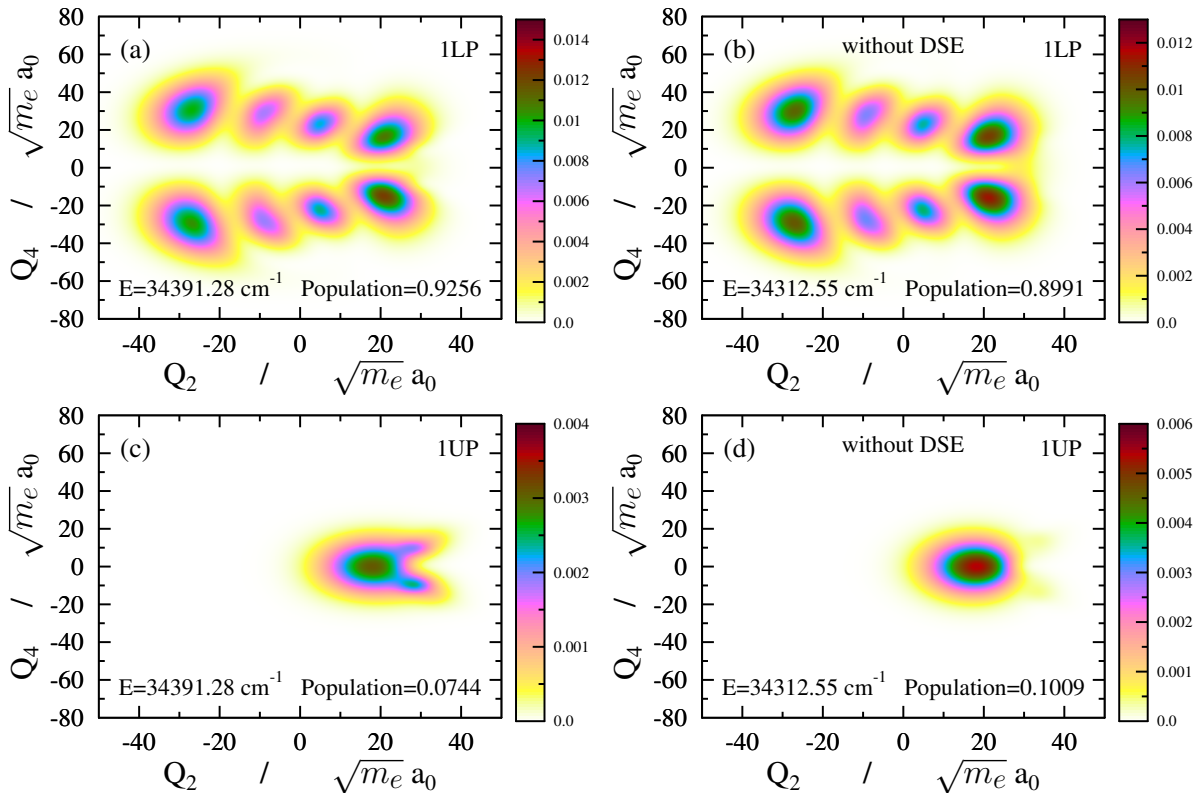


Figure 10: Probability densities (1LP and 1UP states) for cavity-molecule eigenstates populated by laser excitation (panels a and c: with DSE, panels b and d: without DSE). The cavity wavenumber is chosen as  $\omega_c = 34304.93 \text{ cm}^{-1}$  (panels a and c) and  $\omega_c = 34370.27 \text{ cm}^{-1}$  (panels b and d). Other cavity parameters equal  $g = 0.01 \text{ au}$  and  $\mathbf{e} = (1, 1, 1)/\sqrt{3}$ .  $Q_2$  and  $Q_4$  denote normal coordinates of the  $\nu_2$  (C=O stretch) and  $\nu_4$  (out-of-plane) normal modes. Energy levels (given in the figures) are referenced to the lowest energy level. Populations of the 1LP and 1UP states are also given in each panel. Note the similarity between panel pairs in each row.

Next, the laser wavenumber is set to  $\omega = 31389 \text{ cm}^{-1}$  while retaining  $\omega_c = 34304.93 \text{ cm}^{-1}$ .

The corresponding results are presented in Figs. 12, 13 and 14, following the structure of

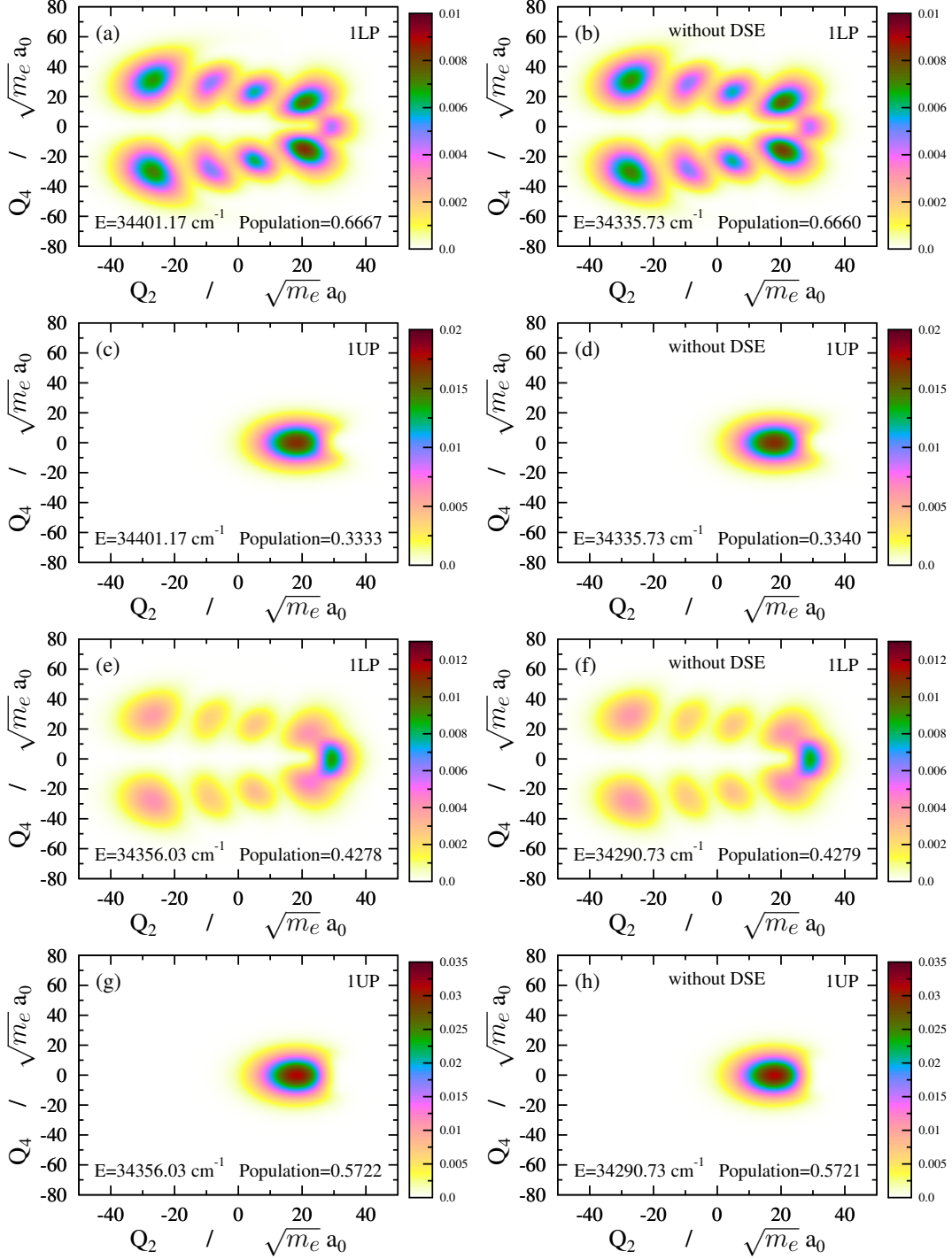


Figure 11: Probability densities (1LP and 1UP states) for cavity-molecule eigenstates populated by laser excitation (panels a, c, e and g: with DSE, panels b, d, f and h: without DSE). The cavity wavenumber is chosen as  $\omega_c = 34370.27 \text{ cm}^{-1}$  (panels a, c, e and g) and  $\omega_c = 34304.93 \text{ cm}^{-1}$  (panels b, d, f and h). Other cavity parameters equal  $g = 0.01 \text{ au}$  and  $\mathbf{e} = (1, 1, 1)/\sqrt{3}$ .  $Q_2$  and  $Q_4$  denote normal coordinates of the  $\nu_2$  (C=O stretch) and  $\nu_4$  (out-of-plane) normal modes. Energy levels (given in the figures) are referenced to the lowest energy level. Populations of the 1LP and 1UP states are also given in each panel. Note the similarity between panel pairs in each row.

results shown previously. In this case, the laser pulse transfers population exclusively to the 1LP polaritonic state. As shown in Fig. 12, results obtained with or without DSE are qualitatively similar although the extent of population transfer is affected. Fig. 13 reveals that dominantly one cavity-molecule eigenstate is populated by the laser with ( $31481.81 \text{ cm}^{-1}$ ) and without ( $31426.70 \text{ cm}^{-1}$ ) DSE, in contrast to the previous resonant case. Moreover, the dominantly-populated eigenstates can be well approximated by A vibrational eigenstates dressed with 0 photons, i.e., the laser excitation targets eigenstates which are not affected by resonant cavity-molecule coupling. Fig. 14 highlights the similarity between the relevant 1LP probability densities of the eigenstates  $31481.81 \text{ cm}^{-1}$  and  $31426.70 \text{ cm}^{-1}$  (both states have negligible 1UP populations).

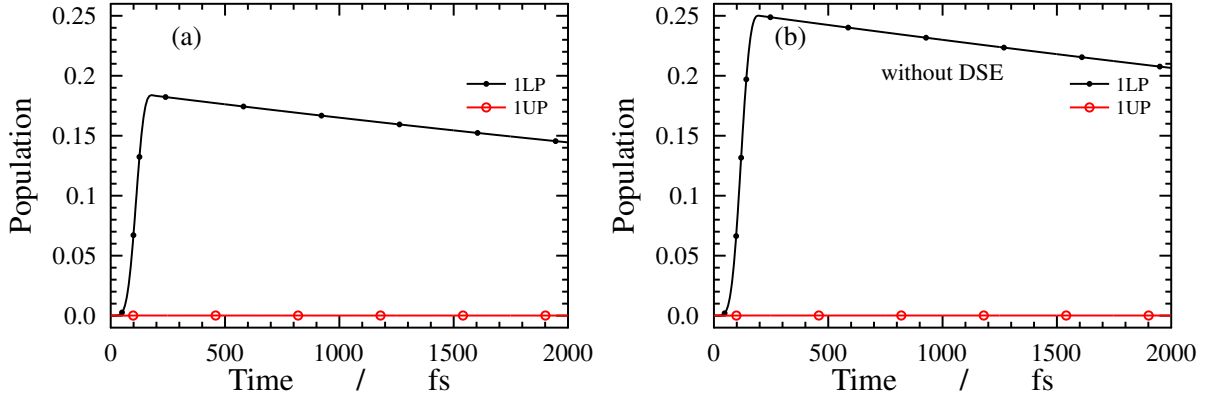


Figure 12: Populations of polaritonic states (1LP and 1UP) as a function of time obtained with (panel a) and without (panel b) the DSE term. Cavity and laser parameters equal  $\omega_c = 34304.93 \text{ cm}^{-1}$ ,  $g = 0.01 \text{ au}$ ,  $\gamma_c = 10^{-4} \text{ au}$ ,  $\mathbf{e} = (1, 1, 1)/\sqrt{3}$ ,  $\omega = 31389 \text{ cm}^{-1}$ ,  $I = 5 \text{ TW/cm}^2$  and  $T = 200 \text{ fs}$ .

## 5 Summary and conclusions

In this paper, we have presented a method for the computation of the dipole self-energy (DSE) term. More precisely, we have implemented the computation of the matrix elements of the squared dipole moment operator ( $(\hat{\mu}\vec{e})^2$  where  $\vec{e}$  is the cavity polarization vector) in the basis of molecular electronic states of interest. In this work, the ground and excited

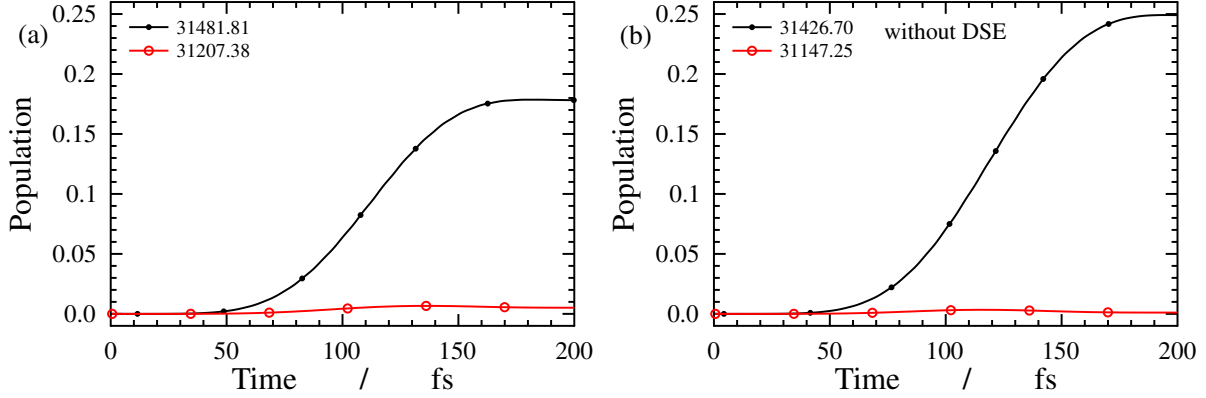


Figure 13: Populations of cavity-molecule eigenstates populated by laser excitation as a function of time (panel a: with DSE, panel b: without DSE). Cavity and laser parameters equal  $\omega_c = 34304.93 \text{ cm}^{-1}$ ,  $g = 0.01 \text{ au}$ ,  $\gamma_c = 10^{-4} \text{ au}$ ,  $\mathbf{e} = (1, 1, 1)/\sqrt{3}$ ,  $\omega = 31389 \text{ cm}^{-1}$ ,  $I = 5 \text{ TW/cm}^2$  and  $T = 200 \text{ fs}$ . Energy levels in the plot legends are given in units of  $\text{cm}^{-1}$  and referenced to the lowest energy level.

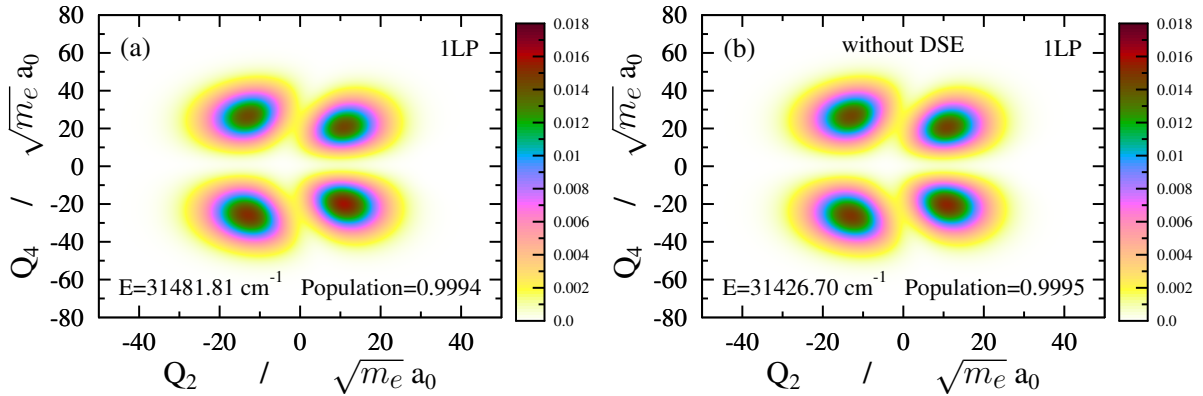


Figure 14: Probability densities (1LP state) for cavity-molecule eigenstates populated by laser excitation (panel a: with DSE, panel b: without DSE). Cavity parameters equal  $\omega_c = 34304.93 \text{ cm}^{-1}$ ,  $g = 0.01 \text{ au}$  and  $\mathbf{e} = (1, 1, 1)/\sqrt{3}$ .  $Q_2$  and  $Q_4$  denote normal coordinates of the  $\nu_2$  (C=O stretch) and  $\nu_4$  (out-of-plane) normal modes. Energy levels (given in the figures) are referenced to the lowest energy level. Populations of the 1LP state are also given in each panel. Note the similarity between panels a and b.

electronic states are described using the RHF and CIS methods which have been found to give sensible results for a two-dimensional vibrational model of the four-atomic formaldehyde molecule. The extension to electronic states computed with more sophisticated approaches should not pose any problem using the proposed method. Our method is similar to the one reported in Ref. 48 where squared dipole moment matrix elements were obtained for the electronic ground state at the RHF level of theory without any further approximations. In addition, our study complements earlier works based on approximating the DSE term with the square of the ground-state dipole moment<sup>98</sup> and using the resolution-of-identity approach to treat the DSE.<sup>97</sup> The latter might require the computation of several electronic states to construct the approximate resolution of identity, while our procedure necessitates only those electronic states which are coupled by the cavity mode (electronic ground state and lowest singlet excited state in the current work).

With electronic structure data needed for the DSE at hand, we have investigated the effect of DSE on cavity-induced nonadiabatic quantum dynamics of a single molecule coupled to a quantized mode of an optical cavity. We have found that inclusion of the DSE in the cavity-molecule Hamiltonian changes both the spatial position and energy of the light-induced conical intersection (LICI) between the 1LP (lower) and 1UP (upper) polaritonic potential energy surfaces in the so-called singly-excited subspace. It has also been shown that the DSE term introduces a slight symmetry breaking which manifests in modifying the LICI position from  $Q_4 = 0$  (without DSE) to  $Q_4 \neq 0$  (with DSE) where  $Q_4$  is the normal coordinate of the out-of-plane mode of formaldehyde. We have presented time-dependent quantum-dynamical results which reflect the nonadiabaticity induced by the cavity. Without the cavity, formaldehyde does not possess conical intersections and its dynamics does not show nonadiabatic effects. The molecule coupled to the cavity is pumped with a laser pulse which transfers population from the lowest cavity-molecule eigenstate primarily to the singly-excited subspace. Although the DSE leads to relatively small shifts in the energy levels and potentials, LICIs are generally sensitive to even small changes of parameters and,

consequently, the populations of the 1LP and 1UP polaritonic states as well as populations of cavity-molecule eigenstates can be rather sensitive to whether or not the DSE is taken into account. However, it is still possible to establish a one-to-one correspondence between cavity-molecule eigenstates obtained with or without the DSE, as demonstrated for eigenstates populated by the laser excitation. We note that small frequency shifts due to the DSE are also related to change in the refractive index.<sup>48</sup> The present investigation is for a single molecule and it would be of interest to extend it to study the impact of the DSE on the dynamics of a molecular ensemble in the cavity.

## Acknowledgement

The authors are indebted to NKFIH for funding (Grant No. K146096). Financial support by the Deutsche Forschungsgemeinschaft (DFG) (Grant No. CE 10/56-1) is gratefully acknowledged. The work performed in Budapest received funding from the HUN-REN Hungarian Research Network. This paper was supported by the János Bolyai Research Scholarship of the Hungarian Academy of Sciences. Supported by the University of Debrecen Program for Scientific Publication.

## References

- (1) Törmä, P.; Barnes, W. L. *Rep. Prog. Phys.* **2015**, *78*, 013901.
- (2) Flick, J.; Ruggenthaler, M.; Appel, H.; Rubio, A. *Proc. Natl. Acad. Sci. U.S.A.* **2017**, *114*, 3026–3034.
- (3) Ribeiro, R. F.; Martínez-Martínez, L. A.; Du, M.; Campos-Gonzalez-Angulo, J.; Yuen-Zhou, J. *Chem. Sci.* **2018**, *9*, 6325–6339.
- (4) Feist, J.; Galego, J.; Garcia-Vidal, F. J. *ACS Photonics* **2018**, *5*, 205–216.

- (5) Flick, J.; Rivera, N.; Narang, P. *Nanophotonics* **2018**, *7*, 1479–1501.
- (6) Hertzog, M.; Wang, M.; Mony, J.; Börjesson, K. *Chem. Soc. Rev.* **2019**, *48*, 937–961.
- (7) Yuen-Zhou, J.; Menon, V. M. *Proc. Natl. Acad. Sci. U.S.A.* **2019**, *116*, 5214–5216.
- (8) Herrera, F.; Owrutsky, J. *J. Chem. Phys.* **2020**, *152*, 100902.
- (9) Garcia-Vidal, F. J.; Ciuti, C.; Ebbesen, T. W. *Science* **2021**, *373*, eabd0336.
- (10) Fregoni, J.; Garcia-Vidal, F. J.; Feist, J. *ACS Photonics* **2022**, *9*, 1096–1107.
- (11) Li, T. E.; Cui, B.; Subotnik, J. E.; Nitzan, A. *Annu. Rev. Phys. Chem.* **2022**, *73*, 43–71.
- (12) Mandal, A.; Taylor, M. A.; Weight, B. M.; Koessler, E. R.; Li, X.; Huo, P. *Chem. Rev.* **2023**, *123*, 9786–9879.
- (13) Bhuyan, R.; Mony, J.; Kotov, O.; Castellanos, G. W.; Gómez Rivas, J.; Shegai, T. O.; Börjesson, K. *Chem. Rev.* **2023**, *123*, 10877–10919.
- (14) Hutchison, J. A.; Schwartz, T.; Genet, C.; Devaux, E.; Ebbesen, T. W. *Angew. Chem. Int. Ed.* **2012**, *51*, 1592–1596.
- (15) Chikkaraddy, R.; de Nijs, B.; Benz, F.; Barrow, S. J.; Scherman, O. A.; Rosta, E.; Demetriadou, A.; Fox, P.; Hess, O.; Baumberg, J. J. *Nature* **2016**, *535*, 127–130.
- (16) Ebbesen, T. W. *Acc. Chem. Res.* **2016**, *49*, 2403–2412.
- (17) Thomas, A.; George, J.; Shalabney, A.; Dryzhakov, M.; Varma, S. J.; Moran, J.; Chervy, T.; Zhong, X.; Devaux, E.; Genet, C.; et al., *Angew. Chem. Int. Ed.* **2016**, *55*, 11462–11466.
- (18) Vergauwe, R. M. A.; George, J.; Chervy, T.; Hutchison, J. A.; Shalabney, A.; Torbeev, V. Y.; Ebbesen, T. W. *J. Phys. Chem. Lett.* **2016**, *7*, 4159–4164.

- (19) Zhong, X.; Chervy, T.; Wang, S.; George, J.; Thomas, A.; Hutchison, J. A.; Devaux, E.; Genet, C.; Ebbesen, T. W. *Angew. Chem.* **2016**, *128*, 6310–6314.
- (20) Chervy, T.; Thomas, A.; Akiki, E.; Vergauwe, R. M. A.; Shalabney, A.; George, J.; Devaux, E.; Hutchison, J. A.; Genet, C.; Ebbesen, T. W. *ACS Photonics* **2017**, *5*, 217–224.
- (21) Groenhof, G.; Toppari, J. J. *J. Phys. Chem. Lett.* **2018**, *9*, 4848–4851.
- (22) Damari, R.; Weinberg, O.; Krotkov, D.; Demina, N.; Akulov, K.; Golombek, A.; Schwartz, T.; Fleischer, S. *Nat. Commun.* **2019**, *10*, 3248.
- (23) Ojambati, O.; Chikkaraddy, R.; Deacon, W.; Horton, M.; Kos, D.; Turek, V.; Keyser, U.; Baumberg, J. *Nat. Commun.* **2019**, *10*, 1049.
- (24) Rossi, T. P.; Shegai, T.; Erhart, P.; Antosiewicz, T. J. *Nat. Commun.* **2019**, *10*, 3336.
- (25) Vergauwe, R. M. A.; Thomas, A.; Nagarajan, K.; Shalabney, A.; George, J.; Chervy, T.; Seidel, M.; Devaux, E.; Torbeev, V.; Ebbesen, T. W. *Angew. Chem. Int. Ed.* **2019**, *58*, 15324–15328.
- (26) Galego, J.; Garcia-Vidal, F. J.; Feist, J. *Phys. Rev. X* **2015**, *5*, 041022.
- (27) Galego, J.; Garcia-Vidal, F. J.; Feist, J. *Nat. Commun.* **2016**, *7*, 13841.
- (28) Kowalewski, M.; Bennett, K.; Mukamel, S. *J. Phys. Chem. Lett.* **2016**, *7*, 2050–2054.
- (29) Flick, J.; Appel, H.; Ruggenthaler, M.; Rubio, A. *J. Chem. Theory Comput.* **2017**, *13*, 1616–1625.
- (30) Herrera, F.; Spano, F. *Phys. Rev. Lett.* **2017**, *118*, 223601.
- (31) del Pino, J.; Schröder, F. A. Y. N.; Chin, A. W.; Feist, J.; Garcia-Vidal, F. J. *Phys. Rev. Lett.* **2018**, *121*, 227401.

- (32) Ruggenthaler, M.; Tancogne-Dejean, N.; Flick, J.; Appel, H.; Rubio, A. *Nat. Rev. Chem.* **2018**, *2*, 0118.
- (33) Szidarovszky, T.; Halász, G. J.; Császár, A. G.; Cederbaum, L. S.; Vibók, Á. *J. Phys. Chem. Lett.* **2018**, *9*, 6215–6223.
- (34) Vendrell, O. *Phys. Rev. Lett.* **2018**, *121*, 253001.
- (35) Mandal, A.; Huo, P. *J. Phys. Chem. Lett.* **2019**, *10*, 5519–5529.
- (36) Mandal, A.; Montillo Vega, S.; Huo, P. *J. Phys. Chem. Lett.* **2020**, *11*, 9215–9223.
- (37) Taylor, M. A. D.; Mandal, A.; Zhou, W.; Huo, P. *Phys. Rev. Lett.* **2020**, *125*, 123602.
- (38) Haugland, T. S.; Ronca, E.; Kjøenstad, E. F.; Rubio, A.; Koch, H. *Phys. Rev. X* **2020**, *10*, 041043.
- (39) Li, T. E.; Nitzan, A.; Subotnik, J. E. *J. Chem. Phys.* **2020**, *152*, 234107.
- (40) Li, T. E.; Subotnik, J. E.; Nitzan, A. *Proc. Natl. Acad. Sci. U.S.A.* **2020**, *117*, 18324–18331.
- (41) Li, X.; Mandal, A.; Huo, P. *Nat. Commun.* **2021**, *12*, 1315.
- (42) Ahrens, A.; Huang, C.; Beutel, M.; Covington, C.; Varga, K. *Phys. Rev. Lett.* **2021**, *127*, 273601.
- (43) Fábri, C. *Mol. Phys.* **2024**, *122*, e2272691.
- (44) Schnappinger, T.; Kowalewski, M. *J. Chem. Theory Comput.* **2023**, *19*, 9278–9289.
- (45) Schnappinger, T.; Kowalewski, M. *J. Chem. Theory Comput.* **2023**, *19*, 460–471.
- (46) Schnappinger, T.; Sidler, D.; Ruggenthaler, M.; Rubio, A.; Kowalewski, M. *J. Phys. Chem. Lett.* **2023**, *14*, 8024–8033.

- (47) Fábri, C.; Császár, A. G.; Halász, G. J.; Cederbaum, L. S.; Vibók, Á. *J. Chem. Phys.* **2024**, *160*, 214308.
- (48) Fiechter, M. R.; Richardson, J. O. *J. Chem. Phys.* **2024**, *160*, 184107.
- (49) Riso, R. R.; Haugland, T. S.; Ronca, E.; Koch, H. *J. Chem. Phys.* **2022**, *156*, 234103.
- (50) Bauer, M.; Dreuw, A. *J. Chem. Phys.* **2023**, *158*, 124128.
- (51) Szidarovszky, T. *Phys. Rev. A* **2023**, *108*, 053118.
- (52) Szidarovszky, T. *J. Chem. Phys.* **2023**, *159*, 014112.
- (53) Aklilu, Y. S.; Varga, K. *Phys. Rev. A* **2024**, *110*, 043119.
- (54) Sandik, G.; Feist, J.; García-Vidal, F. J.; Schwartz, T. *Nat. Mater.* **2024**, in press, DOI: 10.1038/s41563-024-01962-5.
- (55) Wang, D. *J. Phys. B: At. Mol. Opt. Phys.* **2021**, *54*, 133001.
- (56) Du, M.; Martínez-Martínez, L. A.; Ribeiro, R. F.; Hu, Z.; Menon, V. M.; Yuen-Zhou, J. *Chem. Sci.* **2018**, *9*, 6659–6669.
- (57) Li, T. E.; Nitzan, A.; Subotnik, J. E. *Angew. Chem. Int. Ed.* **2021**, *60*, 15533–15540.
- (58) Semenov, A.; Nitzan, A. *J. Chem. Phys.* **2019**, *150*, 174122.
- (59) Mandal, A.; Krauss, T. D.; Huo, P. *J. Phys. Chem. B* **2020**, *124*, 6321–6340.
- (60) Wellnitz, D.; Pupillo, G.; Schachenmayer, J. *J. Chem. Phys.* **2021**, *154*, 054104.
- (61) Campos-Gonzalez-Angulo, J. A.; Ribeiro, R. F.; Yuen-Zhou, J. *Nat. Commun.* **2019**, *10*, 4685.
- (62) Galego, J.; Climent, C.; Garcia-Vidal, F. J.; Feist, J. *Phys. Rev. X* **2019**, *9*, 021057.

- (63) Fregoni, J.; Corni, S. In *Theoretical and Computational Photochemistry*; García-Iriepa, C., Marazzi, M., Eds.; Elsevier, 2023; Chapter 7 - Polaritonic Chemistry, pp 191–211.
- (64) Felicetti, S.; Fregoni, J.; Schnappinger, T.; Reiter, S.; De Vivie-Riedle, R.; Feist, J. *J. Phys. Chem. Lett.* **2020**, *11*, 8810–8818.
- (65) Fregoni, J.; Corni, S.; Persico, M.; Granucci, G. *J. Comput. Chem.* **2020**, *41*, 2033–2044.
- (66) Fregoni, J.; Granucci, G.; Coccia, E.; Persico, M.; Corni, S. *Nat. Commun.* **2018**, *9*, 4688.
- (67) Fregoni, J.; Granucci, G.; Persico, M.; Corni, S. *Chem* **2020**, *6*, 250–265.
- (68) Davidsson, E.; Kowalewski, M. *J. Chem. Phys.* **2020**, *153*, 234304.
- (69) Torres-Sánchez, J.; Feist, J. *J. Chem. Phys.* **2021**, *154*, 014303.
- (70) Fábri, C.; Halász, G. J.; Cederbaum, L. S.; Vibók, Á. *J. Phys. Chem. Lett.* **2024**, *15*, 4655–4661.
- (71) Cederbaum, L. S.; Fedyk, J. *J. Chem. Phys.* **2024**, *161*, 074303.
- (72) Scheel, S.; Buhmann, S. Y. *Acta Phys. Slovaca* **2008**, *58*, 675–809.
- (73) Buhmann, S. *Dispersion Forces I: Macroscopic Quantum Electrodynamics and Ground-State Casimir, Casimir–Polder and van der Waals Forces*; Springer Tracts in Modern Physics; Springer Berlin Heidelberg, 2013.
- (74) Feist, J.; Fernández-Domínguez, A. I.; García-Vidal, F. J. *Nanophotonics* **2021**, *10*, 477–489.
- (75) Power, E. A.; Zienau, S.; Massey, H. S. W. *Philos. Trans. R. Soc. London, Ser. A* **1959**, *251*, 427–454.

- (76) Vukics, A.; Griebner, T.; Domokos, P. *Phys. Rev. Lett.* **2014**, *112*, 073601.
- (77) Woolley, R. G. *Phys. Rev. Res.* **2020**, *2*, 013206.
- (78) Rokaj, V.; Welakuh, D. M.; Ruggenthaler, M.; Rubio, A. *J. Phys. B: At. Mol. Opt. Phys.* **2018**, *51*, 034005.
- (79) Csehi, A.; Halász, G. J.; Cederbaum, L. S.; Vibók, Á. *J. Phys. Chem. Lett.* **2017**, *8*, 1624–1630.
- (80) Csehi, A.; Kowalewski, M.; Halász, G. J.; Vibók, Á. *New J. Phys.* **2019**, *21*, 093040.
- (81) Gu, B.; Mukamel, S. *Chem. Sci.* **2020**, *11*, 1290–1298.
- (82) Gu, B.; Mukamel, S. *J. Phys. Chem. Lett.* **2020**, *11*, 5555–5562.
- (83) Szidarovszky, T.; Halász, G. J.; Vibók, Á. *New J. Phys.* **2020**, *22*, 053001.
- (84) Fábri, C.; Lasorne, B.; Halász, G. J.; Cederbaum, L. S.; Vibók, Á. *J. Phys. Chem. Lett.* **2020**, *11*, 5324–5329.
- (85) Fábri, C.; Lasorne, B.; Halász, G. J.; Cederbaum, L. S.; Vibók, Á. *J. Chem. Phys.* **2020**, *153*, 234302.
- (86) Fábri, C.; Halász, G. J.; Cederbaum, L. S.; Vibók, Á. *Chem. Sci.* **2021**, *12*, 1251–1258.
- (87) Fábri, C.; Halász, G. J.; Cederbaum, L. S.; Vibók, Á. *J. Chem. Phys.* **2021**, *154*, 124308.
- (88) Szidarovszky, T.; Badankó, P.; Halász, G.; Vibók, Á. *J. Chem. Phys.* **2021**, *154*, 064305.
- (89) Farag, M. H.; Mandal, A.; Huo, P. *Phys. Chem. Chem. Phys.* **2021**, *23*, 16868–16879.
- (90) Badankó, P.; Umarov, O.; Fábri, C.; Halász, G. J.; Vibók, Á. *Int. J. Quantum Chem.* **2022**, *122*, e26750.

- (91) Csehi, A.; Vendrell, O.; Halász, G. J.; Vibók, Á. *New J. Phys.* **2022**, *24*, 073022.
- (92) Fábri, C.; Halász, G. J.; Cederbaum, L. S.; Vibók, Á. *Chem. Commun.* **2022**, *58*, 12612–12615.
- (93) Fábri, C.; Halász, G. J.; Vibók, Á. *J. Phys. Chem. Lett.* **2022**, *13*, 1172–1179.
- (94) Fischer, E. W.; Saalfrank, P. *J. Chem. Phys.* **2022**, *157*, 034305.
- (95) Fábri, C.; Csehi, A.; Halász, G. J.; Cederbaum, L. S.; Vibók, Á. *AVS Quantum Sci.* **2024**, *6*, 023501.
- (96) Born, M.; Oppenheimer, R. *Ann. Phys.* **1927**, *389*, 457–484.
- (97) Borges, L.; Schnappinger, T.; Kowalewski, M. *J. Chem. Phys.* **2024**, *161*, 044119.
- (98) Yu, Q.; Bowman, J. M. *J. Chem. Theory Comput.* **2024**, *20*, 4278–4287.
- (99) Yang, J.; Ou, Q.; Pei, Z.; Wang, H.; Weng, B.; Shuai, Z.; Mullen, K.; Shao, Y. *J. Chem. Phys.* **2021**, *155*, 064107.
- (100) Ruggenthaler, M.; Sidler, D.; Rubio, A. *Chem. Rev.* **2023**, *123*, 11191–11229.
- (101) Cohen-Tannoudji, C.; Dupont-Roc, J.; Grynberg, G. *Atom-Photon Interactions: Basic Processes and Applications*; Weinheim (Wiley-VCH Verlag GmbH and Co. KGaA), 2004.
- (102) Schäfer, C.; Ruggenthaler, M.; Rokaj, V.; Rubio, A. *ACS Photonics* **2020**, *7*, 975–990.
- (103) Sidler, D.; Schnappinger, T.; Obzhairov, A.; Ruggenthaler, M.; Kowalewski, M.; Rubio, A. *J. Phys. Chem. Lett.* **2024**, *15*, 5208–5214.
- (104) Angelico, S.; Haugland, T. S.; Ronca, E.; Koch, H. *J. Chem. Phys.* **2023**, *159*, 214112.
- (105) Fischer, E. W.; Saalfrank, P. *J. Chem. Theory Comput.* **2023**, *19*, 7215–7229.

- (106) Visser, P. M.; Nienhuis, G. *Phys. Rev. A* **1995**, *52*, 4727–4736.
- (107) Manzano, D. *AIP Adv.* **2020**, *10*, 025106.
- (108) Mølmer, K.; Castin, Y.; Dalibard, J. *J. Opt. Soc. Am. B* **1993**, *10*, 524–538.
- (109) Jensen, F. *Introduction to Computational Chemistry*; Wiley (Chichester), 2017.
- (110) Alon, O. E.; Cederbaum, L. S. *Phys. Rev. B* **2003**, *68*, 033105.
- (111) Foresman, J. B.; Head-Gordon, M.; Pople, J. A.; Frisch, M. J. *J. Phys. Chem.* **1992**, *96*, 135–149.
- (112) Gerratt, J.; Mills, I. M. *J. Chem. Phys.* **1968**, *49*, 1719–1729.
- (113) Sun, Q.; Berkelbach, T. C.; Blunt, N. S.; Booth, G. H.; Guo, S.; Li, Z.; Liu, J.; McClain, J. D.; Sayfutyarova, E. R.; Sharma, S.; et al., *Wiley Interdiscip. Rev. Comput. Mol. Sci.* **2018**, *8*, e1340.
- (114) Sun, Q.; Zhang, X.; Banerjee, S.; Bao, P.; Barbry, M.; Blunt, N. S.; Bogdanov, N. A.; Booth, G. H.; Chen, J.; Cui, Z.-H.; et al., *J. Chem. Phys.* **2020**, *153*, 024109.
- (115) Meyer, R. *J. Chem. Phys.* **1970**, *52*, 2053–2059.
- (116) Süli, E.; Mayers, D. *An Introduction to Numerical Analysis*; Cambridge University Press, 2003.